Field Trip F 2:

Sediments of the Ries Crater Lake (Miocene, Southern Germany)

Gernot Arp

Geowissenschaftliches Zentrum der Universität Göttingen, Goldschmidtstraße 3, 37077 Göttingen

1. Introduction

The Nördlinger Ries is a circular, flat depression of 22-24 km diameter separating the Jurassic limestone plateaus of the Franconian and Swabian Alb in Southwest-Germany (Fig. 1). Its centre is located 110 km NW of Munich, 70 km SSW of Nuremberg and 110 km E of Stuttgart. The Ries basin was formed approximately 15 Million years ago (Gentner & Wagner, 1969; Staudacher et al., 1982) by an impact of a stony meteorite less than 1 km in size (Shoemaker & Chao, 1961; Stöffler, 1977).

The Ries crater represents one of the best preserved and best investigated impact structures on Earth (Bayerisches Geologisches Landesamt 1969, 1974, 1977; Hüttner & Schmidt-Kaler 1999; Stöffler & Ostertag 1983). It gained wide public attention (e.g., Metz 1974, Steinert 1974, Lemcke 1981, Kavasch 1985, Pösges & Schieber 1994; Schieber 2004) and served as training site for Apollo 17 astronauts in August 1970 (e.g., Margolin 2000).

However, apart from its impact nature, the Ries basin offers a great opportunity to study fossil lacustrine microbialites. Such lacustrine deposits within impact structures are of increasing interest for understanding the origin and evolution of early life on Earth, and possibly other planets (Cockell & Lee 2002, Osinski et al. 2005, Cabrol et al. 2001). Therefore, the focus on this field trip is on microbial and algal build-ups, their facies context, and the discussion of microbial effects and lake water chemistry.

2. The Ries impact

Conclusive evidence for the formation of the Ries basin by a cosmic impact was drawn by Shoemaker & Chao (1961) and Chao & Littler (1963), who discovered the high-pressure polymorphs coesit and stishovit in the suevite, an impact-melt-bearing breccia (Hüttner 1969, 1977). More recently, diamonds and silicon carbide were detected within the suevite (Hough et al. 1995), as well as an ultradense rutile polymorph in shocked gneisses (El Goresy et al. 2001). Today, the following cratering model is generally accepted (Gall et al. 1975, Pohl & Gall 1977):

A stony meteorite with high velocity penetrated through approximately 600 m Jurassic and Triassic sediments down into the crystalline basement rocks of the Moldanubicum. After the vaporization of the projectile and the excavation of a transient crater with a depth of 2 - 2.5 km, gravity caused collapse of the crater rim and uplift of the its floor. The final result was a hydrologically closed, complex impact structure almost 25 km in diameter, subdivided by a ring structure in a central crater and a marginal megablock zone (Reich & Horrix 1955, Chao 1977, Ernstson & Pohl 1977, Stöffler 1977). The ejecta blanket (mainly „Bunte Breccia“) as well as the crater floor was covered by a blanket of the impact-melt bearing crystalline breccia. Today, large parts of the „fallout suevite“ outside the crater are eroded (see Hüttner & Schmidt-Kaler 1999). As a consequence of the gravity modification described above, the later Ries crater lake had a high surface to depth ratio (Fig. 2), if compared to lakes in simple craters.

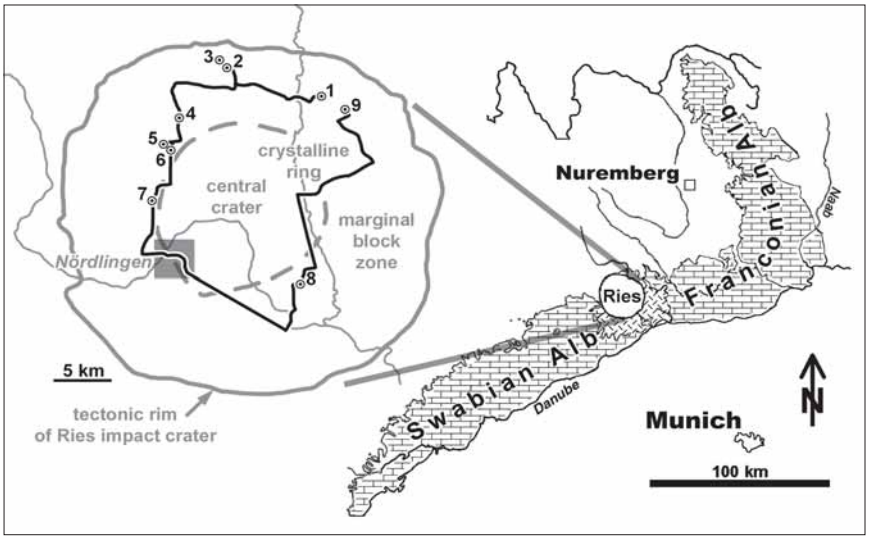

Fig. 1. Location map of the Ries impact crater with excursion route and stops.

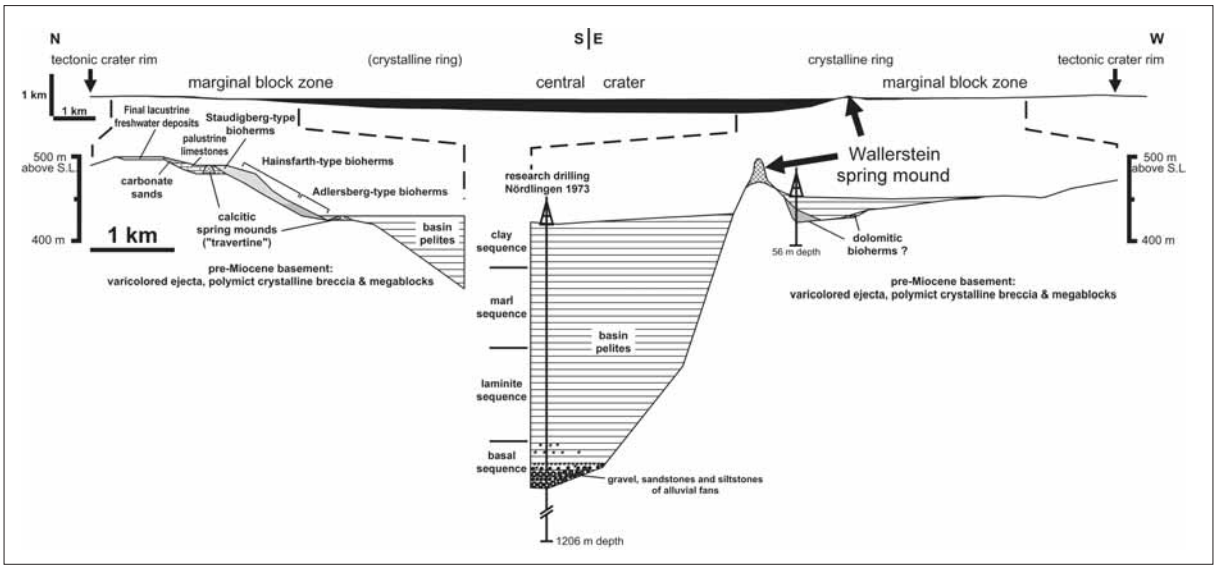

Fig. 2. Cross-section of the Ries crater basin showing major lacustrine facies units. Upper part shows a general section of the shallow basin, divided by a crystalline ring into a central crater and a marginal block zone. Lower part shows two detailed, exaggerated vertical scale sections of the marginal carbonate sediment cover with the location of spring mounds and various bioherms. From Pache et al. (2001), modified.

3. The Miocene Ries crater lake

3.1. Overview on the sedimentary succession

Sediments of the Ries crater lake are preserved within the central basin (more than 300 m, mainly fine-grained clastics) and as erosional remnants (mainly carbonates and coarse-grained clastics) covering hills of the crystalline ring and slopes of the crater rim (Fig. 2; Bayerisches Geologisches Landesamt 1969, Hüttner & Schmidt-Kaler 1999). Large parts of the lake history were documented by the research drilling Nördlingen 1973, which cored a lacustrine sequence of 314.3 m (Bayerisches Geologisches Landesamt 1974, 1977). According to the comprehensive paper of Jankowski (1981), the lacustrine sequence can be divided into four sequences (Fig. 2):

(1) The „basal sequence“ (58.3 m) consists of coarse-grained clastics of alluvial fans, grading into fine-grained carbonate-bearing mudstones of a playa and fossiliferous sediments of a permanent lake.

(2) The following „laminite sequence“ (145 m) shows bituminous dolomitic laminites with abundant diatoms in its upper part. The laminites were deposited during eutrophic and often alkali-saline conditions of a permanent lake with euxinic bottom water.

(3) Sediments of the „marl sequence“ (59 m) are formed by bedded, grey to greenish marls with bioturbation and desiccation structures. Thus, the alternating saline and less saline lake lost its permanent stratification.

(4) Sediments of the „clay sequence“ (52 m) comprise dark-grey, partly carbonaceous clays and thin lignite seams of an episodically non-saline, very shallow lake.

The carbonate and clastic sediments of the Ries crater margins (i.e., the sediments visited during this excursion: Fig. 3) represent the last phase of the Ries lake, thus, are probably younger than the basinal succession described above (see discussion in Jankowski 1981; for contrary view see Wolff & Füchtbauer 1976 and Schauderna 1983). Therefore, more than 100 m of lake basin sediments, which once filled up the complete crater basin, were removed from the central basin since the early Pleistocene (Wolf 1977). The Miocene Ries crater sediments now exposed at the surface can be subdivided into several facies units described below.

3.2. Facies units

Lacustrine clastics of the basin centre

Description: Claystones and marlstones constitute by far the greatest portion of the Ries crater lake sediments (Fig. 2). Permanent surface outcrops, however, do not exist.

The rare temporary surface exposures by construction pits commonly show dark-grey to greenish-grey, laminated claystones with white-grey chalky calcite precipitates forming nodules or coatings on bedding planes (e.g., Wallerstein: Hollaus 1969; Wemding: Bolten et al. 1976; Oettingen: Peters 2003; Trendel: Knollmann 2003). Locally, cm- to dm-thick beds of laminated limestones are intercalated, consisting of micrite and microspar (e.g., Nittingen). Less abundant in the few surface outcrops are blue-grey mas-

sive clays and dark-grey to brownish, bituminous shales (e.g., road-cutting SE of Ehingen). Bituminous shales from drill cores have been shown to contain biomarkers of planktonic green algae (Botryococcan) as well as abundant organic sulfur compounds (Rullkötter et al. 1990; Barakat & Rullkötter (1997). Claystones, oilshales as well as micrite beds locally show slumping structures (Bolten et al. 1976, Mertes 1977, Arp 1995bc). Surprisingly, bedding planes with mud cracks have been observed in these basinal laminites (e.g., Wemding: Bolten et al. 1976).

Most of the basinal sediments are poor in fossils. Hollaus (1969: 20) reported ostracods, few gastropods and fish scales from laminated clays exposed by a sewage plant construction pit at Wallerstein. One exceptional discovery was a fossiliferous bed with numerous fish skeletons and plant remains in laminated clay- and marlstones near Wemding (Bolten et al. 1976).

Interpretation: Laminated clay- and marlstones are considered as profundal sediments of a density-stratified saline lake. However, rare mud cracks in the laminites suggest that water depths were rather shallow and that even central parts of the lake exceptionally suffered temporary desiccation. Bituminous intercalations reflect high primary production of planktonic green algae in the water column and anoxic bottom waters, whereas massive claystones represent intervals of water mixing and bottom water oxygenation. Chalky carbonate precipitates probably resulted from recrystallization of instable primary carbonates and evaporites.

Deltaic clastics of the basin margins

Description: Coarse-siliciclastic deposits related to fluvial influx into the crater lake are known from several localities. They are widespread between Trendel, Ursheim and Megesheim in the NW sector of the Ries basin (Fig. 3), forming the „delta of Trendel“ (Bolten & Müller 1969). Further occurrences are known, e.g., from the Ulrichsberg (stop 5; NE Ries; Groiss 1974), the vicinity of Ederheim (SW Ries; Nathan 1935) and south of Huisheim (SE Ries; Schröder & Dehm 1950).

The sediments comprise coarse conglomerates with cm-sized, poorly to well rounded pebbles within a greenish-grey sandy matrix. Pebbles are commonly 1 to 6 cm in diameter, rarely up to 20 cm. They consist of crystalline rocks or Upper Jurassic limestones, rarely of Middle Jurassic sandstones or kaolinized impact glass. The conglomerate beds form lenticular beds with a poorly visible cross-stratification (Groiss 1974). Conglomerates and sandstones locally interfinger with greenish-grey clayey sandstones and light-grey sandy dolomite beds with root traces, ostracods and *Hydrobia trochulus*.

In the Trendel area, yellow-brownish friable sandstones and ooid-bearing sandstones are widespread (Weber 1941, Bolten 1977). Some of them show a clear cross-stratification and patchy cementation. The latter causes a nodular weathering of the sandstones. Large-scale foreset beds in friable sandstones are exposed in the Megesheim sand pit (stop 9; Chao et al. 1987).

Interpretation: Conglomerates and sandstones are largely deltaic deposits of fluvial inlets into the Ries lake, as already notified by v. Gümbel (1889). Their composition reflects the local availability of pre-Miocene rock types, such as crystalline rocks at the Ulrichsberg and Upper Jurassic limestones in the Ederheim area.

Calcitic spring mounds

Description: Spring mound carbonates, also known as „travertines“ in the Ries basin, form localized mounds and pinnacles with steep sides of meter to several decametre in size (Fig. 2 - 4). Large mounds, such as the Wallerstein (stop 7) and Alerheim castle rocks (stop 8), are commonly located on basement blocks of the crystalline ring structure (Wolff & Füchtbauer 1976; Bolten 1977; Bolten & Gall 1978; Pache et al. 2001). They are up to 30 m high and exhumed from their surrounding lake clays by Pleistocene erosion (Bolten 1977). Further spring

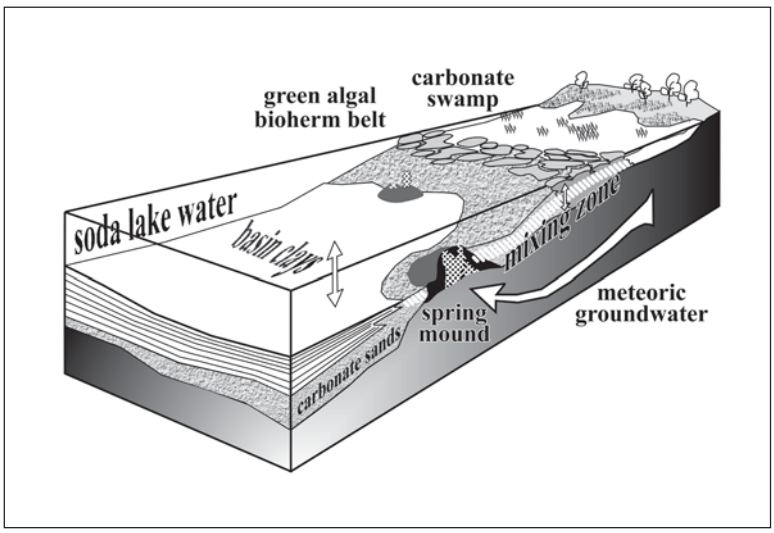

Fig. 4. Reconstruction of the northern Ries lake margin with the distribution of major facies zones. From Arp (1995b).

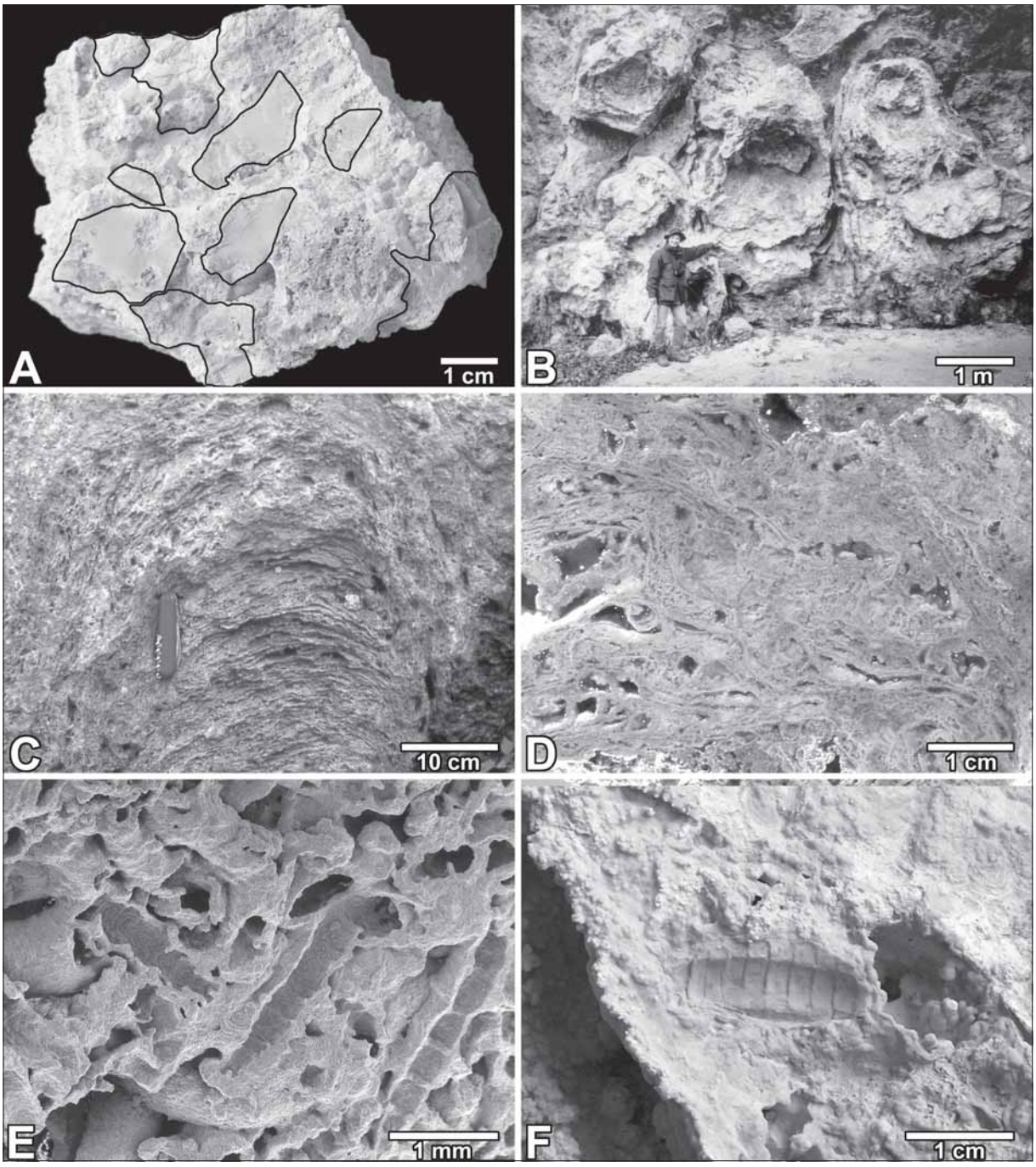

Fig. 5. Spring mound carbonates.
A. Upper Jurassic limestone clasts enclosed in basal spring mound carbonates. Main street, Trendel (Knollmann 2003).
B. Field view of the northern, basal part of the Wallerstein castle rock showing barrel-shaped sickle-cell limestone cones veneered by thrombolite crusts. The core parts of these structures have largely been removed by quarrying. From Pache et al. (2001).
C. Stromatolitic column of sickle-cell limestone at the stairway to the Wallerstein summit.
D. Polished slab of sickle-cell limestone. N of Staudigberg.
E. Pupal cases of flies preserved by passive incrustation at the margin of a spring mound. Leihbug N of Ehingen. SEM micrograph. From Arp (1995b).
F. Negative cast of a dragonfly larva at a sinter-veneered fissure wall of a spring mound. Belzheim.

mounds formed on top of brecciated Upper Jurassic limestones (Fig. 5A) of the marginal megablock zone (e.g., Goldberg; Wolff & Füchtbauer 1976; Bolten 1977), and some few even formed at front parts of deltaic clastics (Weber 1941: p. 130, Abb. 10). Facies mapping revealed that spring mounds are much more widespread that previously through (Fig. 3).

The „travertines“ consist of porous calcitic limestones with only traces of aragonite. In contrasts to the algal

bioherms, microcrystalline dolomite and limpid dolomite cements are absent. Central parts of the mounds and pinnacles (Fig. 5B) are composed of so-called sickle-cell limestones (Fig. 5CD; „Sichelzellenkalke"; Reis 1926). These are highly porous limestones consisting of 100-200 µm thick microcrystalline calcite sheets spanning over mm- to cm-sized lenticular to sickle-shaped voids. Bubble-like structures and networks of micrite threads occur as well (Pache et al. 2001). Laminated and dendroid sinter cements and curtains of thin stalactites, which veneer dissolution voids and fissures, too, stabilize this initial framework.

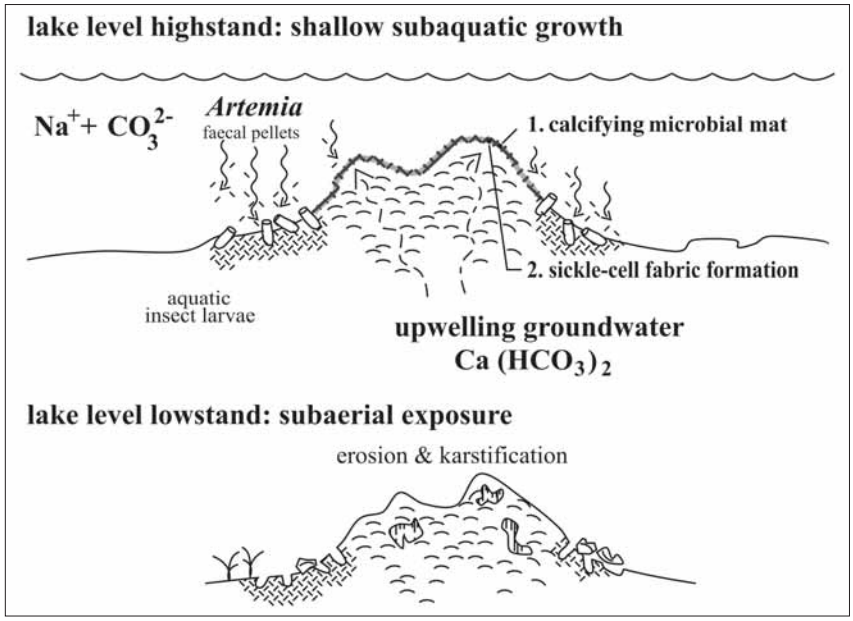

Fig. 6. Model of spring mound formation in the Ries soda lake. Periods of subaquatic growth and prolonged exposure alternated. After initial impregnation of microbial mats within the mixing zone, sickle-cell fabrics form by bacterial degradation and shrinkage of the mats (Arp 1995bc, Arp et al. 1998).

Marginal mound parts show thrombolites, planar non-skeletal stromatolites, and rare green-algal framestones. First lacustrine ostracods and *Hydrobia* shells occur in these marginal mound carbonates, but most characteristic are elongated faecal pellets and insect larval tubes. However, sheet cracks and polygonal mud cracks are common in intercalated non-skeletal stromatolites.

Well-preserved vertebrate remains, such as avian skulls, feather imprints, eggshells and diverse mammals, have been reported from the Ries spring mounds (Deffner & Fraas 1877, Bolten & Müller 1969, Heizmann & Fahlbusch 1983, Kohring & Sachs 1997, Mayr & Göhlich 2004). However, sickle-cell limestones, thrombolites and stromatolites are disappointingly poor in fossils. A closer look to the fossil locations and associated freshwater gastropods suggests that these vertebrate remains are restricted to fissure fillings (e.g., Kohring & Sachs 1997) or mound tops largely belonging to the final freshwater deposits of the Ries lake. Only accumulations of pupal cases of flies (Fig. 5E; Seemann 1935, Arp 1995bc) and larvae of dragonflies (Bolten 1977: 86; Fig. 5F) may coincide in time with the major mound formation.

Interpretation: Spring mounds of the Ries are similar to that of present-day soda lakes such as Mono Lake (Russel 1889, Scholl & Taft 1964), Lake Van (Kempe et al. 1991) and Lake Nuoertu (Arp et al. 1998). These form at sublacustrine springs by mixing of Ca^{2+}-supplying groundwater with bicarbonate-rich alkaline lake water (Fig. 6). As a result, cyanobacterial biofilms flourishing at these spring sites become loosely $CaCO_3$ impregnated due to the extremely high supersaturation of mixing zone waters. Compared to the mixing process, photosynthetic activity is of minor importance in causing $CaCO_3$ precipitation (Arp et al. 1999). However, the characteristic sickle-cell fabric results from exopolymer degradation by heterotrophic bacteria, mucus shrinkage and secondary Ca^{2+} release from the exopolymers (Arp et al. 1998). This process only promotes calcification to form lithified microbialites if the dissolved inorganic carbon of the lake water buffers the simultaneously released CO_2 (Arp et al. 2003). Consequently, sickle-cell fabrics are considered to be indicative of highly alkaline, high-DIC environments, i.e., soda lakes.

Spring mounds growth in the Ries lake basin, however, was affected by lake level fluctuations and recurrent subaerial exposure and karstification during their formation, as indicate by well-developed, multiphasic speleothems (Fig. 6). To date, no evidence has been found that sublacustrine spring waters of the Ries lake basin have been thermal, contrasting with the assumptions of early investigators (v. Gümbel 1870, Klähn 1926, Seemann 1935, 1941). Consequently, the spring mound carbonates are no real travertines, but cool-water tufa deposits (cf. Riding 1991).

Dolomitic algal bioherms

Description: Highly porous algal bioherms are widespread at marginal hills of the Ries basin. They are composed of green algal dolomites, cyanobacterial stromatolites and thrombolites (Reis 1926, Wolff &

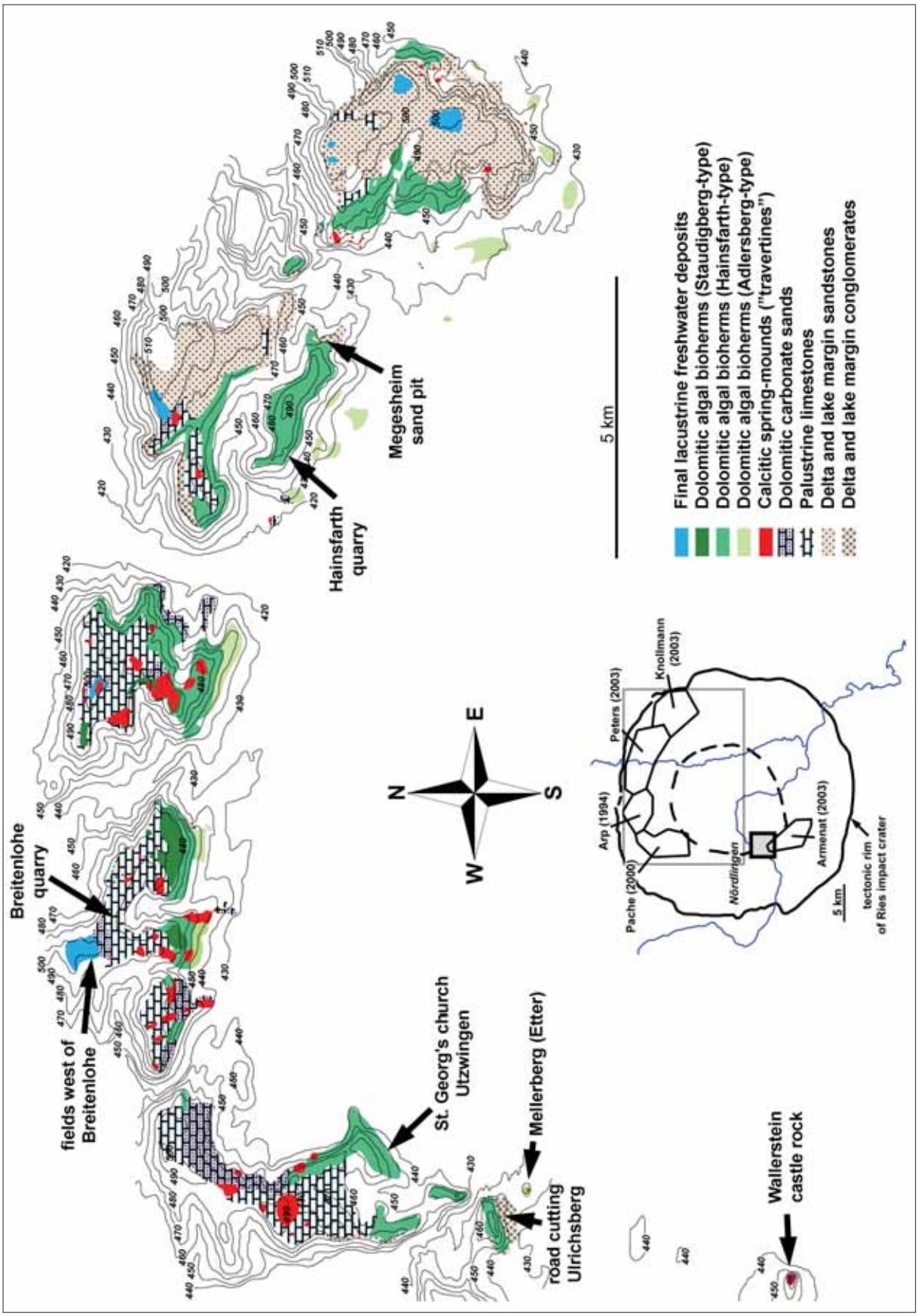

Fig. 3. Facies map of lacustrine and deltaic sediments of the northern margin of the Ries basin. Compiled from Arp (1995c), Pache (2000), Peters (2003) and Knollmann (2003).

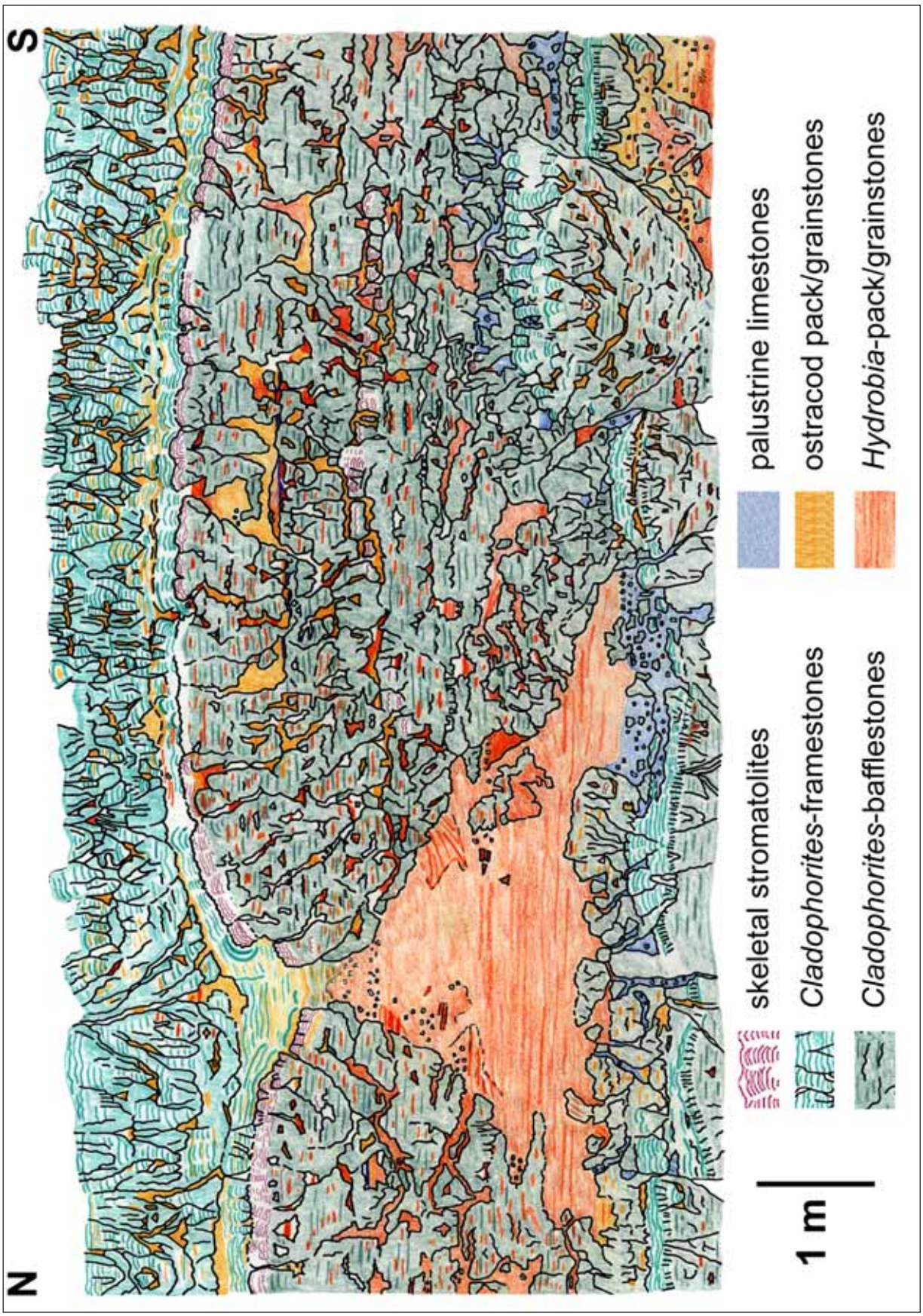

Fig. 12. Facies map of a dolomitic green algal bioherm and associated carbonate sands cross-sectioned at the Hainsfarth quarry at the Büschelberg (Arp 1995bc). Note that black lines indicate laminated sinter veneers, i.e., short-term discontinuities in bioherm growth.

Füchtbauer 1976, Bolten 1977, Riding 1979, Arp 1995bc), which are commonly veneered by rigid, laminated sinter crusts to form nodules, cones and compound cones (stop 1; Riding 1979). The total bioherm succession extends over an elevation difference of 80 m, but the thickness of carbonate deposits at one place rarely exceeds 10 m.

The major bioherm constituent is a fossil green alga closely resembling the modern *Cladophora* (Reis 1926, Wolff & Füchtbauer 1976, Riding 1979. The fossil, termed *Cladophorites incrustatus* (Ludwig) Reis is composed of branching, erect tubes of 50-140 µm inner diameter and dolomicritic walls of 5-15 µm thickness. Pure *Cladophorites*-framestones (Fig. 7A)

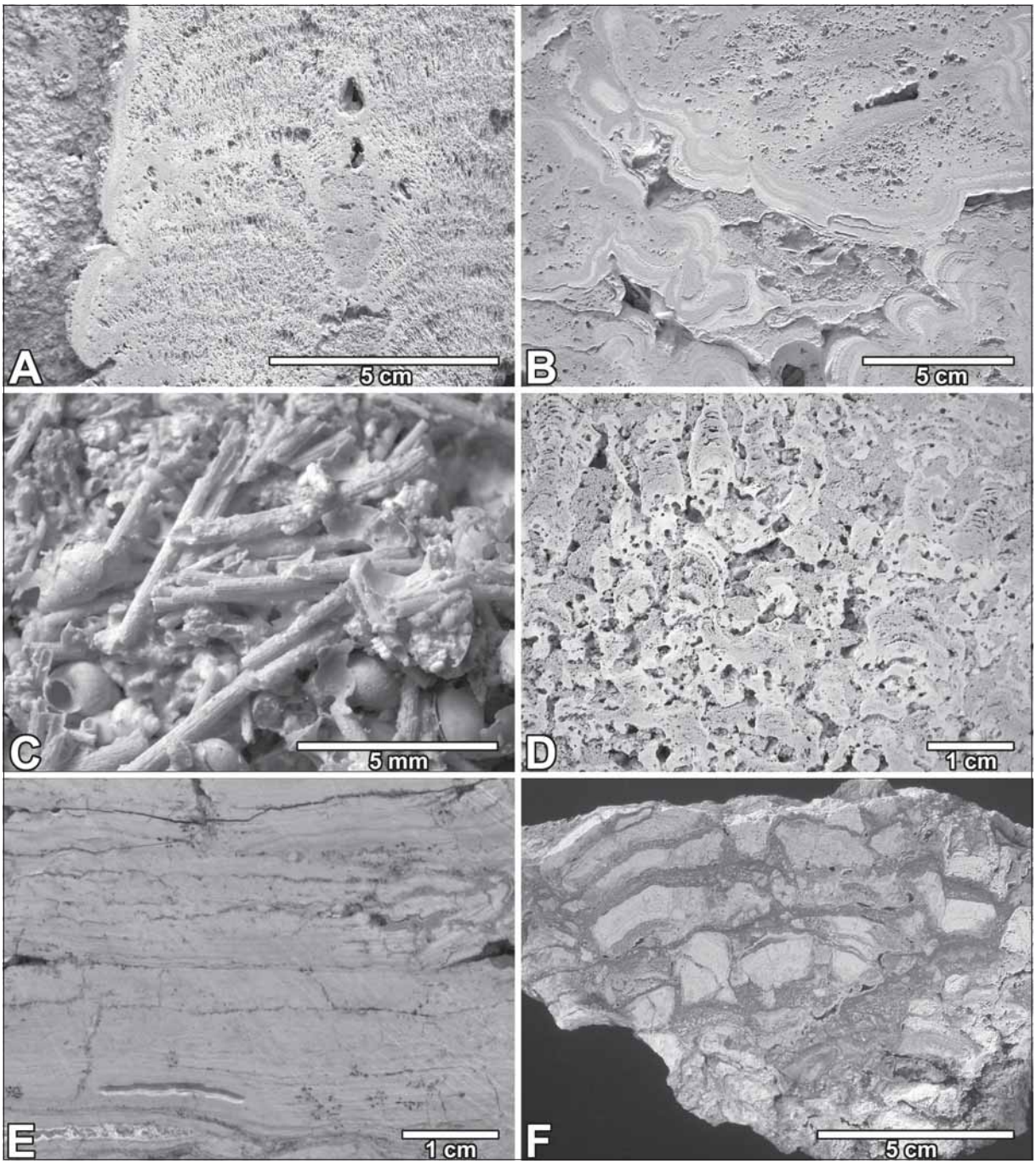

Fig. 7. Algal bioherm carbonates.
A. *Cladophorites*-framestone of a Hainsfarth-type algal bioherm, Ehingen-Lindenstraße.
B. *Cladophorites*-bafflestone of a Hainsfarth-type algal bioherm, NW of Maihingen.
C. Accumulation of charophyte stem fragments in bioherm-associated carbonate sands with *Hydrobia trochulus* and *Strandesia risgoviensis*. Abandoned quarry NNW of Maihingen.
D. Skeletal stromatolite of a Hainsfarth-type algal bioherm, N of Utzwingen. From Pache (2000).
E. Non-skeletal stromatolite, road-cutting Ehingen-Belzheim.
F. *In situ* brecciated stromatolite of a Staudigberg-type algal bioherm. Ehingen Eichenstraße.

exhibit a rhythmic growth pattern due to an alternation of erect tubes and branched, more densely arranged and tangled tubes, while high particle influx results in irregular *Cladophorites*-bafflestones (Fig. 7B). By contrast, charophytes are very rare in the algal bioherms. They are not involved in bioherm growth and occur as poorly calcified, allochthonous stem fragments only. Accumulations of charophyte stem fragments (Fig. 7C), however, have been observed in bioherm-associated carbonate grainstones in the Maihingen-Markoffingen area, which is characterized by co-occurring deltaic conglomerates.

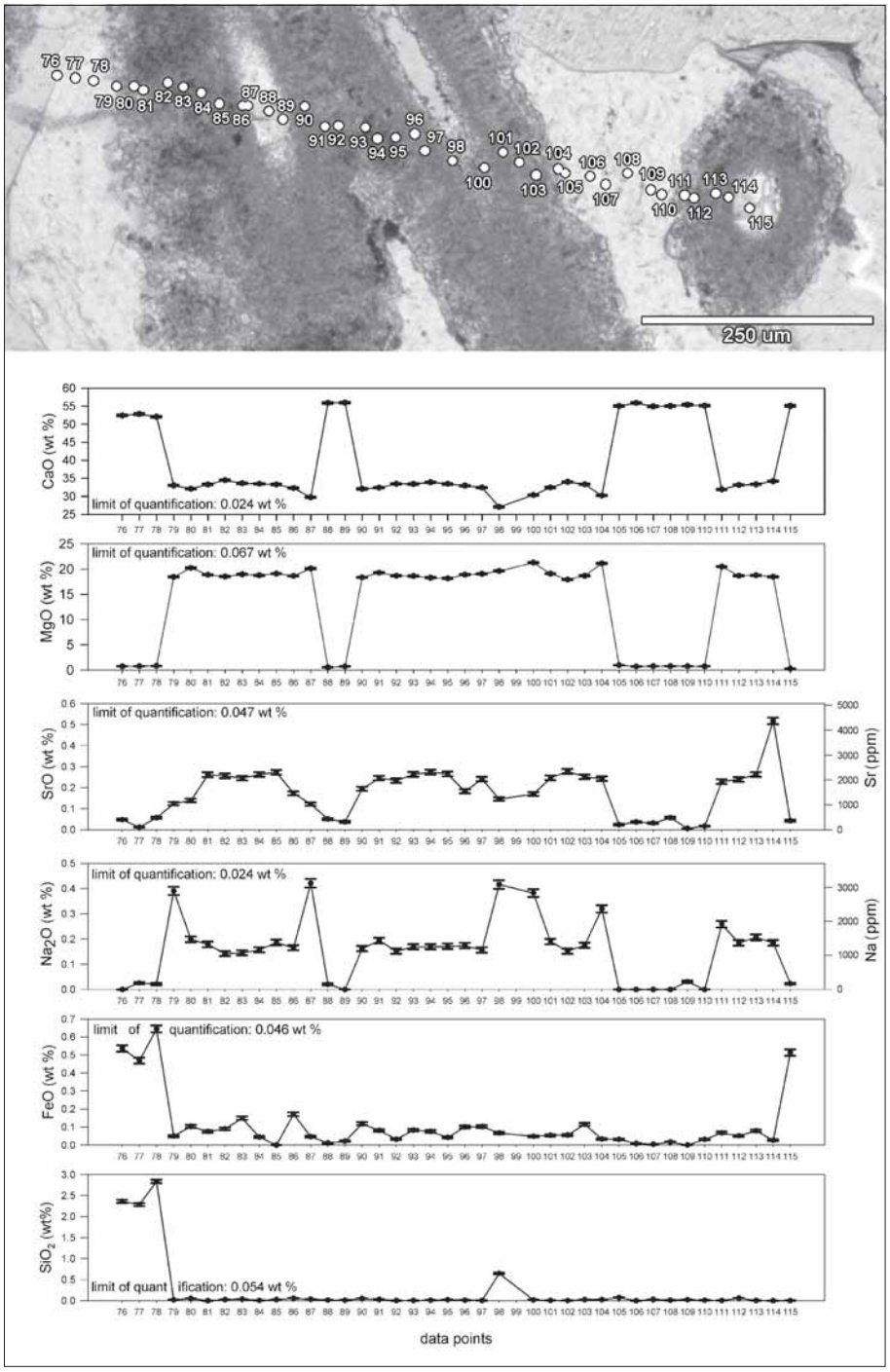

Fig. 8. Electron microprobe analysis of *Cladophorites*-tubes, limpid dolomite cement and late meteoric

Cyanobacterial microfossils are much more rare and restricted to few lithostratigraphic horizons exhibiting skeletal stromatolites (Fig. 7D). Erect filament traces and microcrystalline tubes of 8-12 µm internal diameter may result from former *Oscillatoria*-type cyanobacteria, whereas 1.5- to 2-µm-thin, undulating filaments associated with them may be either cyanobacteria or *Chloroflexus*-type bacteria (Arp 1995bc). Brush-like arranged filament traces of 10-15 µm diameter without defined tube wall might result from *Phormidium*-type cyanobacteria. Coccoid microfossils of possible cyanobacteria, 10-15 µm diameter, have only been detected in one blackened stromatolite clast, redeposited in the palustrine limestones (Peters 2003). By contrast, hollow spheres of 120-130 µm diameter, locally enriched in depressions between stromatolite domes, are arthropod eggs (Arp 1995bc), not coccoid green algae („*Chlorellopsis*“).

Microcrystalline dolomite components of the Ries lake are strikingly rich in Sr (Wolff & Füchtbauer 1976). Apart from that, a limpid dolomite cement consisting of 5-15 µm sized idiomorphic rhombs is present in all of the bioherms. It is less rich in Sr, but shows strikingly high Na concentrations (Fig. 8).

At some segments of the northern rim, the bioherms form an almost continuous „reef belt“ (Fig. 3, 4), while their distribution is more patchy in southern parts of the basin. Numerous small quarries expose these inverted-cone-shaped algal reefs up to a height

of 7 m. Three types of algal bioherms can be distinguished on basis of their facies association:

Adlersberg-type bioherms: These are the oldest known algal bioherms of the Ries basin, occurring as first, patchy bioherm areas covering small hills (stop 6). The type locality Adlersberg quarry shows that the bioherms are composed of green algal dolomite cones and nodules (*Cladophorites*-framestones and -bafflestones) veneered by laminated sinter crusts (Riding 1979). However, the characteristic constituents of Adlersberg-type bioherms are intercalations of planar non-skeletal stromatolites (Fig. 7E), which indicate lake-level lowstands. The bioherm carbonates are associated with bedded skeletal pack- and grainstones, largely composed of the ostracod *Strandesia risgoviensis* (Sieber) (see Janz 1995) and the mesogastropod *Hydrobia trochulus* Sandberger. Pockets within the bioherms locally contain palustrine limestones with accumulations of the land snail *Cepaea sylvestrina* (Schlotheim). Adlersberg-type bioherms show 1 to 3 m thick sedimentary cycles, represented by an alternation of nodular to conical green algal dolomites and planar non-skeletal stromatolites (Riding 1979, Jankowski 1981).

Hainsfarth-type bioherms: This type of bioherms is younger than the Adlersberg-type bioherms and represents the maximum distribution of algal bioherms in the Ries basin (stop 1). At the northern margin of the Ries basin, Hainsfarth-type bioherms form an almost continuous bioherm belt between Maihingen and the „delta of Trendel“ (Fig. 3). Similar to Adlersberg bioherms, Hainsfarth-type bioherms are mainly composed of green algal dolomite cones and nodules (*Cladophorites*-framestones and -bafflestones) veneered by laminated sinter crusts (Riding 1979; Arp 1995bc; Fig. 7AB). Again, the bioherms are associated with bedded pack- and grainstones composed of ostracods (*Standesia risgoviensis*), mesogastropods (*Hydrobia trochulus*), ooids, peloids and intraclasts. Likewise, pockets of palustrine limestones with abundant *Cepaea sylvestrina* are common. Exceptional findings are thin-walled foraminifera, one specimen of the freshwater gastropod *Brotia escheri*, and a dolomitized millipede (Arp 1995abc).
In contrast to Adlersberg-type bioherms, planar non-skeletal stromatolites do not occur any more. Instead, skeletal stromatolites (Fig. 7D) are developed at the top of bioherm cycles, just below discontinuities. These stromatolites are increasingly abundant to the top of the Hainsfarth-type bioherm succession. Here, skeletal stromatolites and stromatolite-incrusted wood fragments form a lithostratigraphic marker bed.

Hainsfarth-type bioherms show a clear cyclic facies development (Fig. 9): Palustrine limestones with *Cepaea sylvestrina* are the first deposits of a cycle, commonly preserved in pockets of the preceding bioherm cycle. Bioherm growth starts with nodular *Cladophorites*-bafflestones, followed by cones of rhythmically grown *Cladophorites*-framestones, and further nodular *Cladophorites*-bafflestones. Cycle tops are characterized by skeletal stromatolites, subsequent erosion and pocket formation.

Staudigberg-type bioherms: These are the youngest known algal bioherms of the Ries basin, occurring as relictic deposits at the northern basin margin near Ehingen (e.g., Staudigberg) and Oettingen (e.g.,

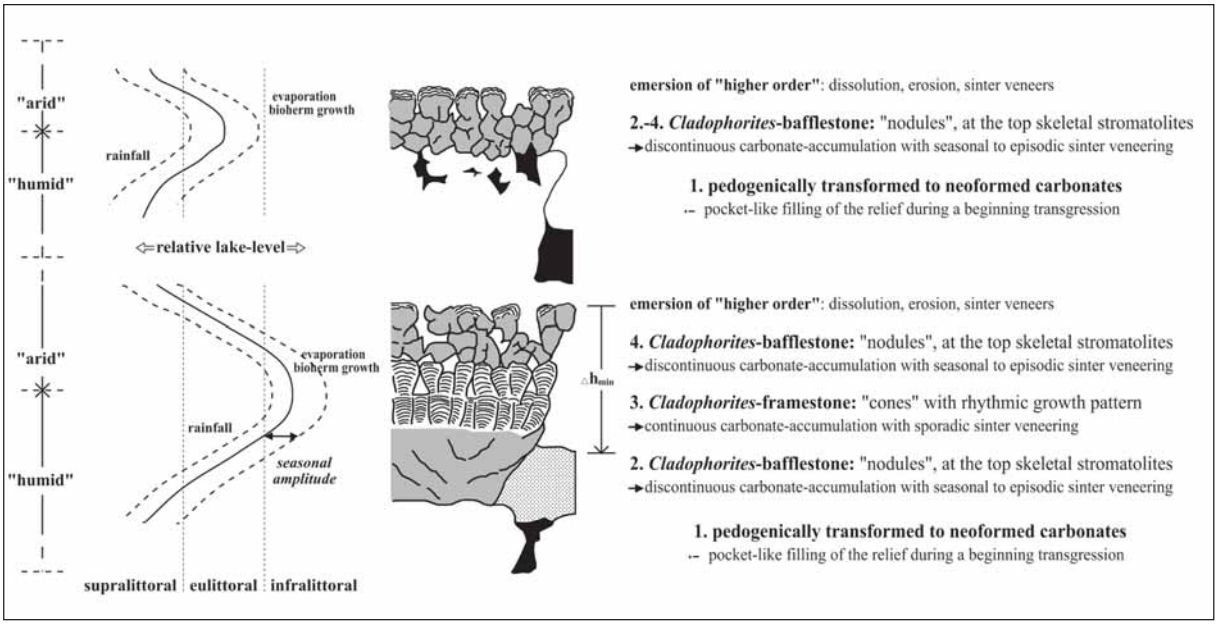

Fig. 9. Cycle scheme of Hainsfarth-type algal bioherms. Lake level fluctuations due to short-term climatic changes are shown simplified by a sinus-like graph. Complete sequences are 1.5-2.5 m thick. From Arp (1995b).

Affenberg). Previously, these bioherms have been described as intraclastic carbonates forming an „aragonitic top horizon“ (Wolff & Füchtbauer 1976). However, temporary outcrops in Ehingen revealed that major parts of the lithologic unit are microbialite bioherms brecciated *in situ* by pedogenesis (Arp 1995bc). Most striking are white, aragonite-bearing, brecciated stromatolites (Fig. 7F) within a peloidal, greenish-grey to brownish calcite matrix. Limpid dolomite cements are still present. In addition, grey, aragonite-bearing thrombolites are a major component of the 0.5 to 1 m thick bioherm cycles. In contrast to previous bioherms, green algal dolomites (*Cladophorites*-baffle/framestones) do not occur any more. *Hydrobia trochulus* and ostracods are rare.

Interpretation: Dolomitic algal bioherms of the Ries lake occupy large parts of the former lake shore. In contrast to spring mounds, there is to date no evidence of groundwater influx that possibly supported calcification in the bioherms. The cyclic development of the bioherms apparently reflects evaporation-driven lake level fluctuations due to short-term climatic fluctuations, because the Ries lake had no outlet at that time.

Sinter-veneered *Cladophorites*-bafflestones probably formed by high-Mg calcitic impregnation of biofilms upon green algal filaments and baffling of allochthonous particles between the resulting tubes within the wave-exposed eulittoral. Primary aragonite precipitates were present, too, but were of minor importance. The laminated sinter crusts, characterized by pendent morphologies, are interpreted to be of lacustrine-vadose origin. Prolonged eu- to supralittoral conditions are reflected by non-skeletal stromatolites and skeletal stromatolites. On the other hand, intervals of lake level highstand and shallow sublittoral conditions allowed undisturbed, rhythmic growth of *Cladophorites*-framestones. These *Cladophorites* growth rhythms are considered to reflect seasonal rhythms and suggest average annual accumulations of 4 mm for framestones. Assuming that *Cladophorites*-bafflestones grew only half as fast as the framestones because of seasonal exposure, a 2 m thick bioherm composed of frame- and bafflestones may have grown within only 800 years. The bioherm-affecting short-term climatic cycles may therefore represent time intervals of several hundred to a few thousands of years. Conversely, much longer time periods may be represented by subaerial exposure and non-deposition. Dolomitization including dolomite cement precipitation was clearly phreatic and has been related to evaporative lake level fluctuation (Wolff & Füchtbauer 1976, Arp 1995bc). However, the exact mechanism (mixing zone dolomitization, seepage reflux, microbial) remains to be elucidated.

Dolomitic carbonate sands

Description: Coarse bedded pack- and grainstones lithified by limpid dolomite, fibrous calcite and blocky calcite cements are commonly associated with algal bioherms. However, where bioherm are patchy or absent (e.g., Herblingen-Hochaltingen area), these carbonate sands constitute a separate facies unit (Fig. 3). This is also true for the transition to final freshwater deposits of the Ries lake, where algal bioherms are completely absent (e.g., Loher Kopf plateau and south of Breitenlohe; Fig. 2, 3).

Most common facies types are ooid-grainstones, peloid-packstones with root traces (Fig. 10A), intraclast- and oncoclast- rudstones (Fig. 10B). However, ostracod-pack/grainstones and *Hydrobia*-pack/grainstones dominate at lithostratigraphic levels equivalent to Hainsfarth-type bioherms. *Cepaea* shells are commonly broken into bioclasts and bored by endolithic algae. Locally, carbonate sands show a clear cross-stratification (e.g., Alerheim, Arp & Wiesheu 1997). In early lithostratigraphic levels, carbonate sands are associated with non-skeletal stromatolites that form the transition to spring mounds (e.g., road cutting Ehingen-Belzheim; Arp 1995bc). Later lithostratigraphic levels show pedogenically modified pack- and wackestones, i.e. palustrine limestones, instead.

Similar to algal bioherms, dolomitic carbonate sands show a cyclic succession. Pack- and grainstones alternate with erosional discontinuities or platy dolomite mudstones with polygonal mud cracks (Fig. 10C). The latter appear to be restricted to lithostratigraphic levels equivalent to Adlersberg-type bioherms.

Interpretation: Dolomitic carbonate sands are the dominant lake shore deposits, between algal bioherms and where algal bioherms are absent (e.g., transition to final lacustrine freshwater deposits). While peloid-packstones with well preserved root traces (Fig. 10A) characterize shallow sublittoral conditions, skeletal pack/grainstones as well as intraclast- and oncoclast-rudstones are considered as deposits of a wave-exposed eulittoral. Non-skeletal stromatolites and palustrine limestones finally represent supralittoral plains. Climatic fluctuations causing prolonged lake-level lowstands and playa conditions are indicated by dolomite mudstones with mud cracks (Arp 1995bc, Arp & Wiesheu 1997).

Palustrine limestones

Poorly bedded limestones occur at the backside of the dolomitic algal bioherm belt, especially at the northern rim of the Ries basin (stop 2; Fig. 3-5). They interfinger with the bioherms, forming pocket and fissures fillings within them. Locally, greenish-grey marl intercalations have been observed, too. Palustrine

limestones are composed of calcitic mud- and wackestones that show complex desiccation cracks (Fig. 10D), dissolution-enlarged root traces, animal burrows and *in situ* formed grains (nodules, pedogenic ooids, pisoids). Complex desiccation cracks include skew planes, curved planes and craze planes (see Freytet & Plaziat 1982). Some of these crack systems show multiple sinter cement generations and an inverse gradation of intraclasts formed *in situ* (Fig. 10D). The land snail *Cepaea sylvestrina* (Schlotheim) is very common in palustrine limestones. In addition to that, other pulmonate gastropods occur as well, such as *Discus (Discus) costatus* (Gottschick) and *Granaria antiqua noerdlingensis* (Klein) (Bolten 1977, Arp 1995bc).

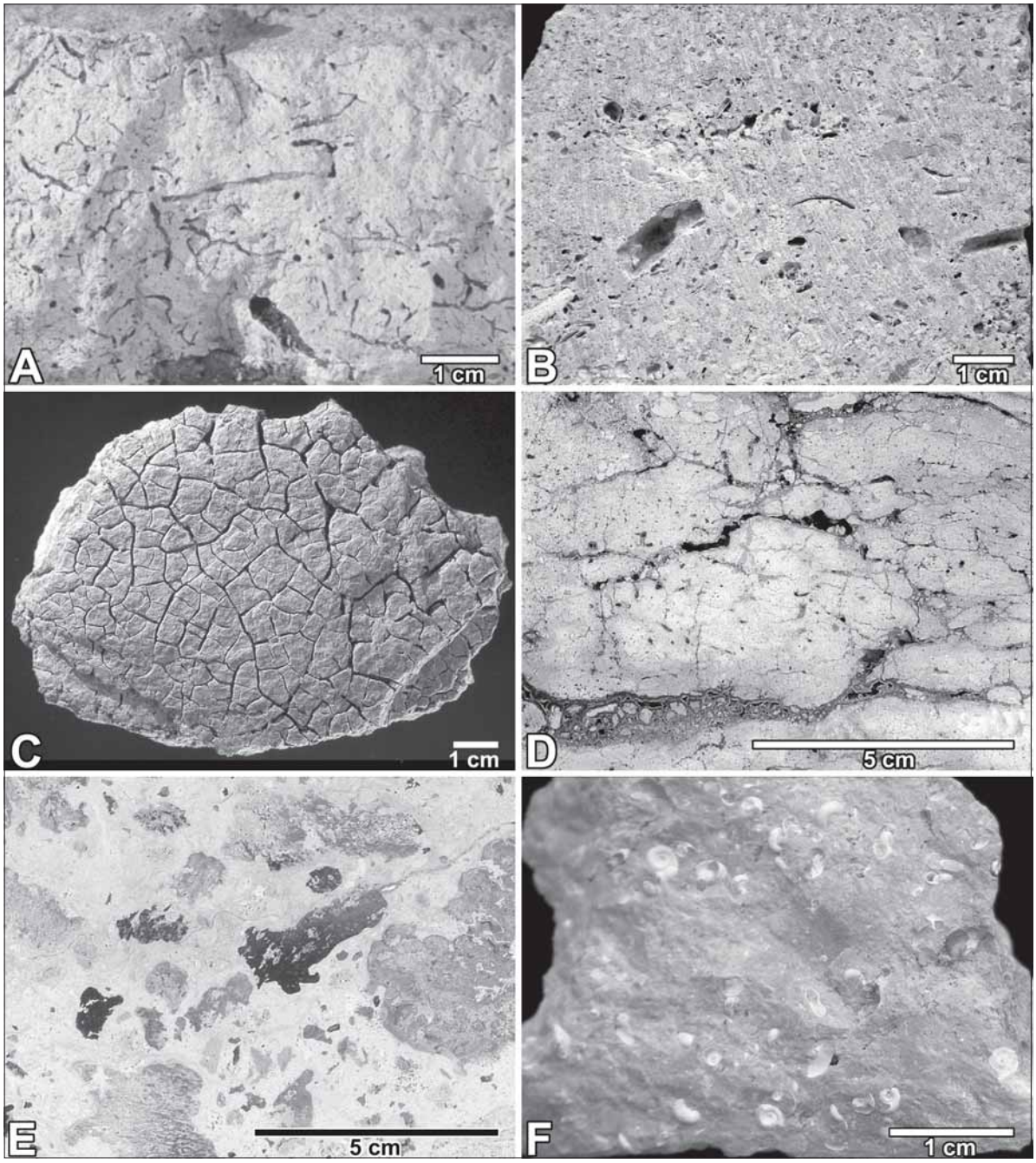

Fig. 10. Dolomitic carbonate sands, palustrine limestones and final lacustrine freshwater deposits.
A. Shallow sublittoral peloid-packstone with root traces. Road-cutting Ehingen-Belzheim.
B. Intraclast-oncoclast-rudstone of the wave-exposed eulittoral. Road-cutting Ehingen-Belzheim.
C. Platy dolomicrite with polygonal mudcracks of playa intervals. Alerheim village. From Arp & Wiesheu (1997).
D. Palustrine limestone with complex desiccation cracks and abundant intraclasts. Abandoned quarry W of Loher Kopf. From Peters (2003).
E. Polished slab of black-pebble-conglomerate. Blackened and unaltered bioherm clasts are embedded in a pedogenic matrix with caliche-like crusts. Höllbug NW of Ehingen.
F. Bioturbated ostracod-wackstone rich in the freshwater gastropod *Gyraulus kleini*. Final lacustrine freshwater deposits WSW of Breitenlohe.

A peculiar facies type within the palustrine facies unit are black pebble rudstones (Fig. 10E), previously described as „algal nodule limestones“ (Bolten 1977; see also Andres 1952). These are conglomeratic limestones with blackened bioherm clasts up to 12 cm diameter (skeletal stromatolites, *Cladophorites*-baffle/framestones) embedded in pedogenic peloidal micrite. Pebbles show multiple incrustations by brownish, indistinctly laminated crusts of pedogenic origin (Caliche). These crusts locally contain the microproblematicum *Limnocodium*, which is a variety of *Microcodium* known from paleosols (Klappa 1978, Freytet & Plaziat 1982). Black pebble rudstones were found up to 300 m behind the bioherm belt and show a patchy distribution. They probably form dm-thick intercalated beds between palustrine limestones.

Interpretation: Palustrine limestones represent a calcareous swamp or floodplain behind the algal bioherm belt (Arp 1995bc). Dissolution-enlarged root traces, complex desiccation cracks, *in situ* formation of grains and vadose cements point to a common alternation of flooding, swamp pedogenesis and subaerial exposure (see Freytet & Plaziat 1982). Black pebble rudstones are interpreted as deposits of episodic storm and flooding events that caused transport of bioherm clasts to elevated, exposed areas of the floodplain (Arp 1995bc). Here, prolonged subaerial exposure and paleosol formation caused blackening and caliche formation.

Final lacustrine freshwater deposits

Description: Only relictic deposits of this latest period of the Ries crater lake history are preserved. These are patchy remnant occurrences at high topographic levels at the northern and northeastern basin margin (Bolten 1977, Arp 1995bc; Fig. 2, 3). Furthermore, a number of marly fissure and pocket fillings of the Goldberg spring mounds belong to these youngest Ries lake sediments (Bolten 1977).

Near Breitenlohe, final freshwater deposits comprise greenish-grey marls and clays with intercalated light-grey limestones bed (stop 3). These are bioturbated ostracod wackestones with root traces, freshwater gastropods, and poorly calcified charophyte remains. Within marls and marly limestones, gastropods still show their primary, aragonitic mineralogy (Fig. 10F). Most abundant freshwater gastropods are *Gyraulus kleini* (Gottschick & Wenz), *Radix socialis dilatata* (Noulet) and *Planorbarius cornu mantelli* (Dunker). It is noteworthy that *Gyraulus kleini* (Fig. 10F), which shows an intra-lacustrine speciation in the contemporaneous Steinheim crater lake (Hilgendorf 1866, Mensink 1984, Gorthner 1992), does not show any evolutionary changes in the Ries crater lake.

Other localities further east (i.e., Loher Kopf, northeast of Kreuzhof, top beds of the „delta of Trendel“ near Ursheim) comprise light-grey to yellow-brownish quartz-rich oolites and calcareous sandstones. The deposits show gastropod faunas with *Gyraulus kleini* (Gottschick & Wenz), *Radix socialis dilatata* (Noulet), *Planorbarius cornu mantelli* (Dunker), *Melanopsis kleini kleini* Kurr, *Theodoxus crenulatus crenulatus* (Klein), *Valvata radiatula radiatula* Sandberger, and few unionid bivalves (Bolten 1977). However, temporary increased salinities are indicated by co-occurrence of the mesogastropod *Hydrobia trochulus* Sandberger at some the localities (Bolten 1977).

In contrast to earlier deposits of the Ries crater lake, sediments of the final freshwater stage commonly show vertebrate remains (Bolten 1977). Also, fissure and pocket fillings at the top of spring mounds appear to belong to this late freshwater stage of the Ries crater lake. These deposits revealed remains of cyprinid fish, salamanders, tortoises, lizards, birds (among them ducks, cranes, parrots, pelicans and flamingo-related birds), and mammals (among them hedgehogs, rodents, hares, bats, and even-toed hoofed mammals; Deffner & Fraas 1877, Seemann 1941, Bolten & Müller 1969, Ballmann 1979, 1983, Heizmann & Fahlbusch 1983, Ziegler 1983, Rachl 1983, Heizmann & Hesse 1995) associated with freshwater gastropods (Bolten 1977).

Interpretation: The marls, limestones and calcareous sandstones described above are considered as shallow sublittoral to low-energy eulittoral deposits of a final freshwater stage of the Ries crater lake. This final freshening period may have been caused by climatic change (increase in humidity, decrease in temperatures) and/or formation of an outlet (Wolff & Füchtbauer 1976, Bolten 1977, Arp 1995bc).

3.3. Palaeoenvironmental interpretation and present-day analogues

Long species lists of fossils described from the Ries lake deposits, especially those from spring mound localities, suggest a generally hostile freshwater environment for the crater lake. However, large parts of the siliciclastic succession in the central basin recovered by the research drilling Nördlingen 1973 show rather species-poor lacustrine fossil assemblages (Dehm et al. 1977). Only early parts (e.g., at 262 m core depth) and intervals near the top of the drilled sequence (less than 52 m core depth) provide evidence of reduced salinities and temporary freshwater conditions (Füchtbauer et al. 1977, Dehm et al. 1977, Jankowski 1977, 1981). The laminite

sequence, characterized by oil shales and autigenic minerals known to form under highly-alkaline conditions (analcime and clinoptilolite), apparently was deposited in a stratified soda lake (Jankowski 1981). Also, covariation of stable oxygen and carbon isotopes provide evidence for a hydrologically closed basin (Rothe & Hoefs 1977).

Marginal carbonates of the Ries basin, considered by Jankowski (1981: 197) to be younger than the central lake deposits recovered by the drillings (e.g., Nördlingen 1973, Deiningen 1 and 2), are characterized by a strikingly species-poor but individual-rich fossil association. This is especially true for Adlersberg- and Hainsfarth-type bioherms and associated carbonate sands. The dominance of one ostracod species (*Strandesia risgoviensis*) and one mesogastropod species (*Hydrobia trochulus*) and the lack of freshwater molluscs indicate saline, probably brackish conditions.

Increased alkalinities are indicated by sickle-cell limestones of the spring mounds. Today, such fabrics only form at sublacustrine spring sites of highly-alkaline salt lakes, i.e. soda lakes such as Lake Van in Anatolia (Kempe et al. 1991), Mono Lake in California (Russel 1889, Scholl & Taft 1964) and Lake Nuoertu in the Inner Mongolia (Arp et al. 1998). Mass accumulations of pupal cases of flies preserved at the Ries spring mounds (Seemann 1935, Arp 1995bc) are also well known from various present-day halite and soda lakes. Lower parts of the marginal carbonates, i.e., Adlersberg-type bioherms and stratigraphic equivalents, even show intercalations of playa sediments and traces of former evaporite minerals.

Besides of cyanobacteria, algal bioherms are dominated by only one green algal genus related to the extant *Cladophora*. This alga is well known to flourish under phosphate- and nitrate-rich conditions. This observation fits to the restriction of charophytes, which prefer nutrient-poor freshwater to oligohaline conditions, to carbonates nearby deltaic deposits.

Skeletal stromatolites with coarse laminated fabrics, that characterize top parts of Hainsfarth-type bioherms, resemble that of Lake Thetis and Lake Clifton in Western Australia (Moore 1987, Grey et al. 1990). These lakes are alkaline salt lakes with ion ratios similar to seawater. From this point of view, the sporadic occurrence of one foraminiferal species within Hainsfarth-type bioherms is less surprising.

Youngest bioherms (i.e., Staudigberg-type bioherms) are increasingly affected by swamp pedogenesis. The lack of calcareous algal tubes in these bioherms probably reflects decreasing $CaCO_3$ supersaturation due to increased humidity and dilution of lake waters, finally leading to freshwater deposits with poorly calcified charophytes.

In conclusion, the marginal Ries lake carbonates reflect the development from a eutrophic soda lake, successively turning into a more Ca^{2+}-rich salt lake (with a pronounced seasonality), and finally into an oligotrophic Ca^{2+}-rich freshwater lake. This general development is superposed by short-term climatic fluctuations causing bioherm cycles, and seasonality causing annual sedimentary rhythms.

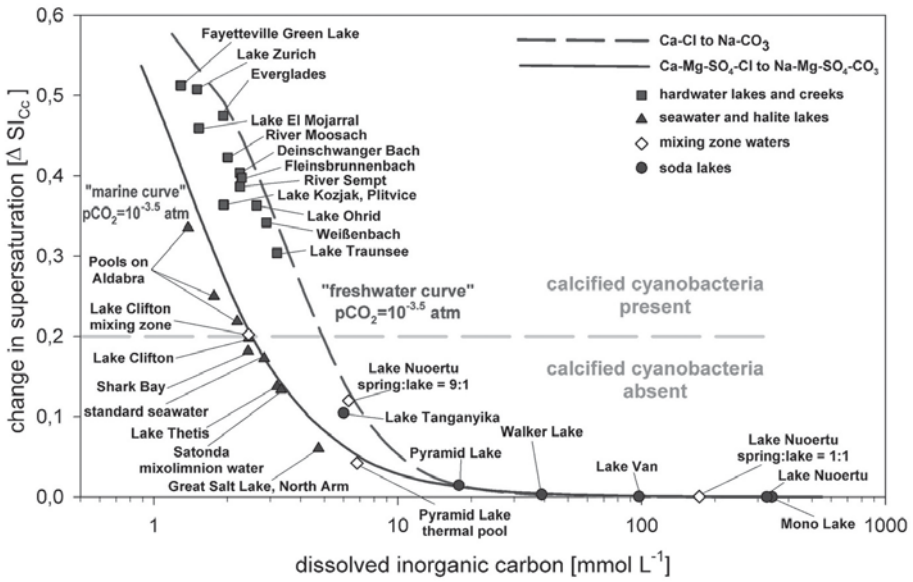

Fig. 11. Computed effect of carbon assimilation on the $CaCO_3$ supersaturation of natural waters as a function of carbonate alkalinity for present-day atmospheric pCO_2 (Arp et al. 2001). The y-axis indicates the resulting change in the supersaturation index (SI_{cc} = log (IAP/K_{so}) denoted as DSI_{cc}. High-alkalinity waters (i.e., soda lakes) show only minor changes in $CaCO_3$ supersaturation upon carbon removal, whereas low-alkalinity waters (i.e., hardwaters) are strongly affected.

3.4. Lacustrine microbialites and seawater chemistry

The algal bioherm succession of the Ries basin show a replacement of non-skeletal stromatolites (lacking calcareous cyanobacterial microfossils) by skeletal stromatolites (with calcareous cyanobacterial microfossils) concomitant to the successive change from soda lake to halite salt lake and finally freshwater conditions (Arp 1995bc). Although a relation of cyanobacterial

calcification to changes in lake water chemistry was obvious, the exact mechanisms explaining this observation remained unclear.

Following investigations of biofilm calcification in present-day lakes and model calculations demonstrated that cyanobacterial photosynthesis causes calcareous tubular microfossils only in Ca^{2+}-rich and poorly pH-buffered settings (Fig. 11; Arp et al. 2001). This relation reflects the solubility product and pH buffering by the dissolved inorganic carbon pool. Consequently, calcareous cyanobacterial microfossils can be used to trace secular changes in seawater Ca^{2+} throughout the Phanerozoic when taking into account paleo-partial pressure curves for carbon dioxide (Arp et al. 2001). In turn, the enigmatic lack of calcified cyanobacteria in stromatolite-bearing Precambrian sequences can now be explained as a result of high dissolved inorganic carbon concentrations (Arp et al. 2001). With regard to the Ries basin, the formation of calcareous cyanobacterial tubes within the skeletal stromatolites points to increasing Ca^{2+}-concentrations and decreasing alkalinities during the late history of the crater lake.

As a further consequence, secondary Ca^{2+} release from bacterial degradation of biofilm exopolymers effectively causes $CaCO_3$ precipitation only when the simultaneously released CO_2 is buffered by high dissolved inorganic carbon concentrations. Therefore, the sickle-cell limestones, which reflect calcification during biofilm degradation, CO_2 release and associated shrinkage, are characteristic of soda lakes (Arp et al. 1998, 2003). Similar fabrics related to biofilm degradation occur in fenestrate microbialites of the Late Archaean („cuspate microbialites“ with vertical supports and draping laminae; Sumner 1997) and may reflect high seawater alkalinities similar to that of soda lakes.

4. Post-Miocene history

At the end of the Miocene the Ries crater basin was completely filled by lacustrine sediments (Bolten & Müller 1969). This view is supported by the degree of coalification in lignite seams in the clay sequence of the research drilling Nördlingen 1973 (Wolf 1977: 135f.). Since that time, more than 100 m lacustrine sediments have been removed from the central basin, largely during the Pleistocene. The central erosional plain of the exhumed crater is now at 420-430 m above S.L., which is 100-150 m lower than the bordering hills of the morphological rim.

Tectonic movements caused a minor tilting of the whole region to the northeast. This is evident, e.g., by tilting of Lower Miocene marine Molasse sediments (Obere Meeresmolasse) south and southwest of the Ries, and highest occurrences of *Hydrobia*-bearing sediments within the Ries basin (see discussion in Bolten 1977). The tectonic movements may have started already late in Miocene times and possibly persisted into Pleistocene times (Bolten 1977).

Meanwhile facies mapping of lacustrine carbonates revealed that the bioherm succession at southern Ries margin (Armenat 2003) is indeed 25 m higher in altitude that at the northern margin (Arp 1995b, Pache 2000, Peters 2003, Knollmann 2003). Possible first movements late in Miocene times may have caused a more widespread freshwater deposition at the northern Ries margin, while equivalent freshwater sediments further south were restricted to pockets of emerging spring mound carbonates.

5. Description of the stops

Stop 1: Hainsfarth quarry at the Büschelberg (7029 Oettingen i.Bay., east 44 00 050, north 54 25 000).

It is the largest and best-known outcrop of dolomitic algal bioherms and associated carbonate sands (Fig. 12). Three adjacent abandoned quarries provide exposures more than 330 m long and up to 7 m high (Riding 1979). The outcrop has previously been described by v. Gümbel (1889, 1891), Wolff & Füchtbauer (1976), Bolten (1977), Jankowski (1981) and is visited by almost any Ries excursion (e.g., Hüttner et al 1996, Hüttner & Schmidt-Kaler 1999, Groiss et al. 2000, Schieber 2002, Höfling 2003). However, the carbonates are still commonly termed „freshwater limestones“, although most of them are dolomites (Klähn 1926, Nathan 1926) deposited in an alkaline salt lake (Bolten 1977, Jankowski 1981, Arp 1995bc).

The first comprehensible description and drawing of the outcrop section has been provided by Riding (1979). Several one to two meter thick sequences of fused green algal nodules and cones compose loaf-shaped dolomitic bioherms up to 15 m across. Bedded carbonate sands consisting of peloids, ostracods (*Standesia risgoviensis*) and gastropods (*Hydrobia trochulus*) form irregular channels in between. The bioherms are subdivided by discontinuities associated with sinter veneers of stalactitic appearance (Fig. 7B), delineating pockets and channels of skeletal sands (Riding 1979). Thus, these laminated crusts are not cyanobacterial stromatolites but lacustrine-vadose precipitates due to evaporation-forced calcification of biofilms (Arp 1995bc).

Detailed facies mappings of quarry walls elucidated cyclic bioherm growth, discontinuities (erosion,

dissolution and sinter veneering), and complex timely relations between algal carbonates and associated skeletal sand of pockets and channels (Fig. 12). Complete bioherm cycles, e.g., as seen in basal parts of the Hainsfarth quarries, show the following facies sequence (Fig. 9):

(1) First deposits are palustrine limestones, either rich in bioherm clasts of previous cycles or extraclasts of the pre-Miocene basement (e.g., the breccia of Jurassic limestones at the basis of the Hainsfarth section). Common are root traces and moulds of *Cepaea sylvestrina*.

(2) Bioherms start with nodules and indistinct cones of *Cladophorites*-bafflestones rich in mesogastropods, dissolution voids and laminated sinter crusts indicating common subaerial exposure events in the wave-exposed eulittoral (Fig. 7B).

(3) Cones of *Cladophorites*-framestone with abundant ostracods, few dissolution voids and thin sinter veneers represent maximum flooding and shallow sublittoral conditions (Fig. 7A).

(4) A further bed of nodular *Cladophorites*-bafflestones with mesogastropods and dissolution voids follows, with increasingly thick sinter veneers. This points to a decrease in lake level and an increasing abundance of subaerial exposure events.

(5) Skeletal stromatolites formed during eu- to supralittoral conditions are locally developed on top of the cycle (Fig. 7D).

(6) Finally, the cycle ends with a prolonged subaerial exposure, erosion and formation of sinter veneers.

The next cycle starts with palustrine limestones with bioherm fragments, root voids and *Cepaea sylvestrina* in erosional pockets and fissures of the completed bioherm cycle (Fig. 9). Further three, reduced, cycles form the main part of the bioherms in Hainsfarth, followed by two undulating bioherm beds at the outcrop top (Fig. 12). These cycles show an increasing portion of skeletal stromatolites, which become widespread at the already poorly exposed outcrop rim.

Strikingly, the contact between algal bioherm carbonates and skeletal sands is always discontinuous and marked by sinter veneer (Fig. 12). This means that skeletal sands are always younger than the adjacent bioherm carbonate. Facies mapping of quarry walls shows that ostracod-rich framestones correlate with ostracod-rich pocket fillings 0.3 to 1 m below them, suggesting a syndepositional relief. Thus, ostracods were deposited in already sinter-veneered pockets and fissures of previous bioherm cycles. The depth of erosional pockets filled with palustrine carbonates indicate long-term lake level fluctuations in the order of 1 to 2.5 m (Fig. 9), while seasonal fluctuations may have been less (Arp 1995bc).

Stop 2: Breitenlohe quarry (7029 Oettingen i.Bay., east 43 93 600, north 54 27 400).

Palustrine carbonates are exposed with up to 2,4 m thickness in this abandoned field quarry 400 m SSE of Breitenlohe (Arp 1995bc). The yellow to white-grey, instinct bedded limestones show dissolution-enlarged root voids (1-3 mm diameter), complex desiccation cracks (Fig. 13) and scattered pulmonate gastropods (*Cepaea sylvestrina*). Coarse bedding is caused by less resistant limestone layers or intercalations of porous intraclasts.

The microfacies is characterized by pedogenically neoformed nodule-ooid-wackestones with root voids and animal burrows. Only at the outcrop base pedogenically neoformed nodule-wackestones with skew planes are developed (Fig. 13). They show grey micritic patches due to soft pebbles and bioturbation („striotubules“).

Stop 3: Fields west of Breitenlohe (7029 Oettingen i.Bay., east 43 93 100, north 54 27 750).

The fields west of the village Breitenlohe constitute the largest relict occurrence of final freshwater deposits of the Ries crater lake. A detailed map and description of this occurrence has been provided by Bolten (1977).

Lower parts of the freshwater deposits are ochre-coloured calcareous marls with a diverse freshwater gastropod fauna, described by Bolten (1977) from a temporary trench. On top of them, white-grey weathered, loose limestone plates with abundant *Gyraulus kleini* follow, which are widely distributed on the fields (Fig. 10F). Marly limestones with aragonitic shells of *Gyraulus kleini*, *Radix socialis dilatata* and *Planorbarius cornu mantelli* are much more rare. At the northern end of the freshwater limestone occurrence, a narrow E-W trending strip with intraclast-rich marly micrites containing disarticulated carapaces of the tortoise *Testudo* sp. was found (Arp 1995bc).

Stop 4: St. Georg’s church Utzwingen (7029 Oettingen i.Bay., east 43 90 175, north 54 23 675).

This fortified church is largely built of algal carbonates from quarries nearby. The porous but rigid dolomitic algal bioherm carbonates once formed one of the few suitable building stones in the Ries area, aside from the partially melted impact breccia suevite. There are no documents on the age of this church, but remains of ancient, now closed windows suggest a construction in the twelfth to late thirteenth century. The

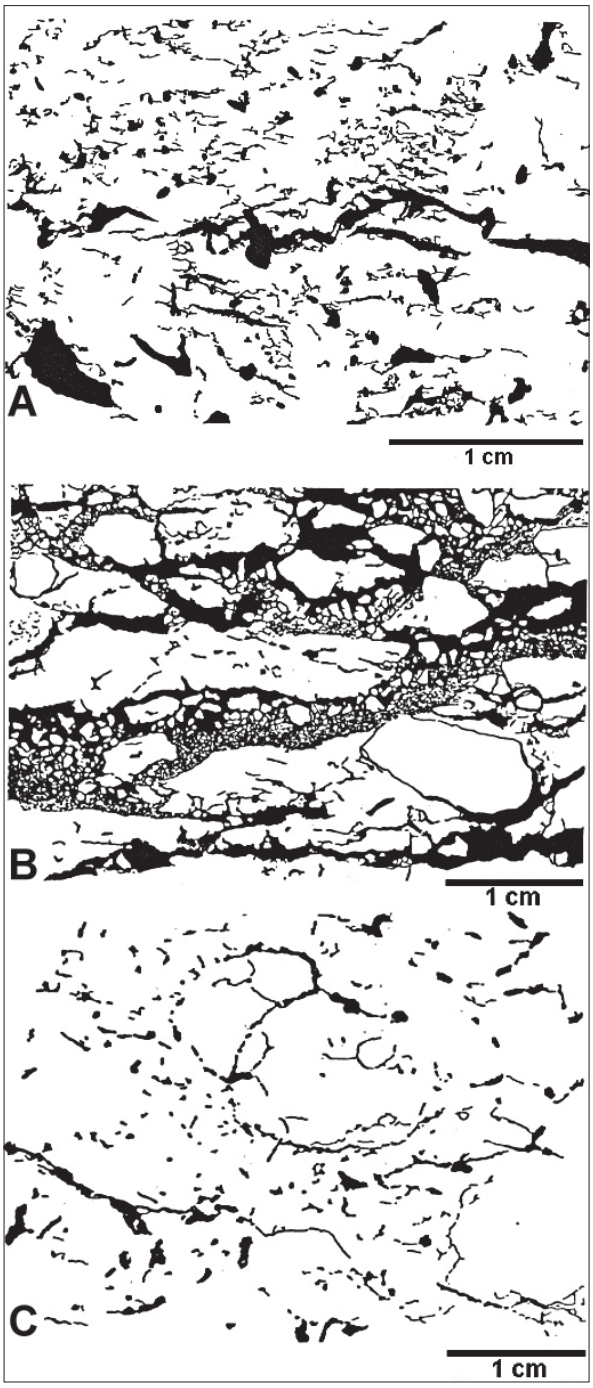

Fig. 13. Complex desiccation cracks in palustrine limestones.
A. Skew planes. Breitenlohe quarry.
B. Craze planes with inverse gradation. N of Staudigberg.
C. Curved planes. N of Staudigberg. From Arp (1995b).

present large windows probably originated in baroque time. More recently, Pleistocene travertine was used for repair of the walls at few places. At the small parking lot in front of the church, a basin made of dolomitic algal bioherm carbonates can be seen at a water pump. The cutting planes excellently show nodular *Cladophorites*-bafflestones with laminated sinter veneers and pockets in-between. In addition, several Christian crosses cut from algal bioherm dolostones excavated during a pipeline construction near Maihingen are visible in this rural commune.

Stop 5: Road-cutting Ulrichsberg (7028 Unterschneidheim, east 36 09 000, north 54 22 000).

The road-cutting exhibits 4 m of bedded, coarse conglomerates and greenish-grey, clayey sandstones resting on impact-brecciated crystalline basement rocks (Fig. 14, 15). These conglomerates consist of cm-sized crystalline rock pebbles and are interpreted as deposits of a deltaic inlet into the Ries lake. The conglomerates form lenticular beds with a poorly visible cross-stratification directed to southern directions, as formerly exposed in a gravel pit north of the road cutting (Groiss 1974). Few, thin beds of light-grey, sandy dolomites with root traces and the mesogastropod *Hydrobia trochulus* are intercalated, indicate a transition to dolomitic carbonate sands of the lake shore. To top of the succession, the transition to dolomitic algal bioherms, which cover the Ulrichsberg, is poorly exposed (Fig. 14, 15). Noteworthy is an 80 cm-thick conglomeratic bed near the outcrop basis, which shows dm-sized algal bioherm fragments, *Cladophorites*-tufts and *Hydrobia trochulus*. These components demonstrate that bioherm formation was contemporaneous with fluviodeltaic influx.

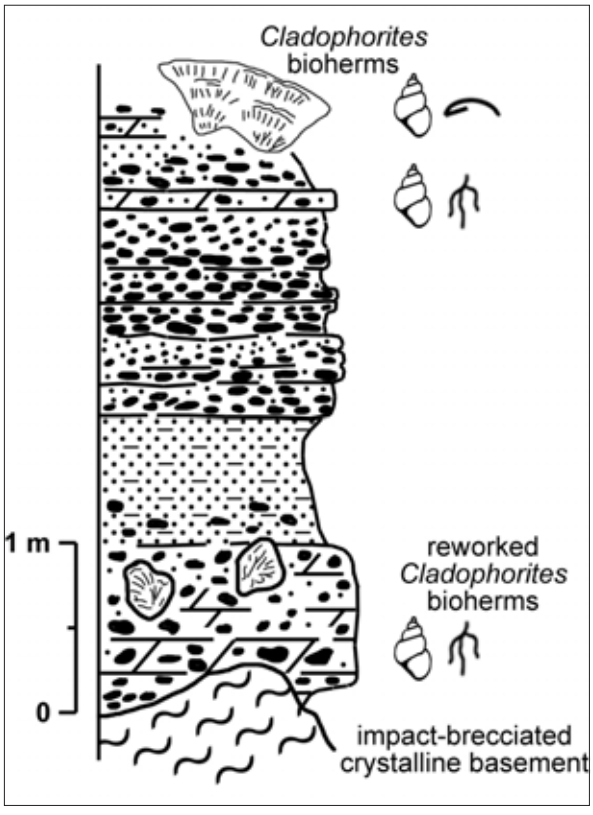

Fig. 14. Lithologic log of the fluviodeltaic conglomerates exposed in the road-cutting Ulrichsberg W of Maihingen.

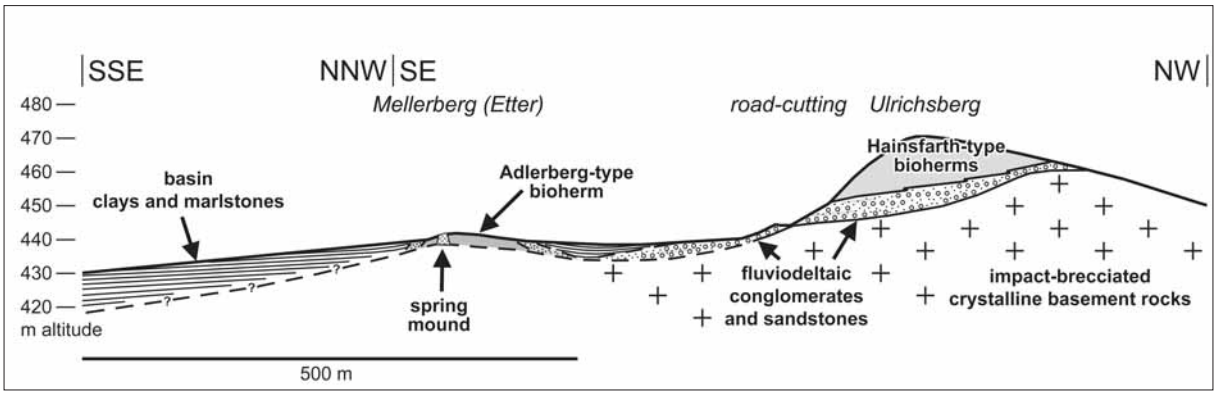

Fig. 15. Geological cross-section of the Mellerberg–Ulrichsberg area showing the position of fluviodeltaic conglomerates, algal bioherms and spring mounds.

Stop 6: Mellerberg (7028 Unterschneidheim, east 36 09 450, north 54 21 675).

The Mellerberg („Etter") is a small hill southwest of the road-cutting Ulrichsberg, already located within the Ries plain (Fig. 15). It exhibits dolomitic algal bioherms (Wolff & Füchtbauer 1976) associated with fossiliferous pack/grainstones (*Strandesia risgoviensis*, *Hydrobia trochulus*) and non-skeletal stromatolites. However, new exposures during the construction of a cycleway (alongside the road from Maihingen to Birkhausen) demonstrated that this Adlersberg-type algal bioherm exhibits a spring mound in its centre. Sickle-cell limestone boulders excavated during this roadwork are now placed beside of the cycleway.

Stop 7: Wallerstein castle rock (7128 Nördlingen, R 36 08 450, H 54 17 430)

This hill is one of the largest spring mounds in the Ries basin, forming a conspicuous rock upon the crystalline ring structure of the crater (Fig. 2). Crystalline rocks of the pre-Miocene basements have been drilled below *Strandesia*- and *Hydrobia*-rich carbonates 670 m west of the castle rock (Nathan 1957). The castle rock attains a height of 495.6 m of above sea level, thereby surpassing the surrounding Ries plain by 70 m. Approximately 30 m of „travertine" are exposed due to quarrying during the twelfth to nineteenth century (Diemand, 1898).

Most parts of the Wallerstein are composed of sickle-cell limestones (Reis 1926), i.e., highly porous limestones characterized by irregular, wavy laminae enclosing lenticular to sickle-cell-shaped voids (Fig. 5C, 16). At the northside base of the castle rock, such limestones form the cores of steep-sided pinnacles up to 4.5 m height, which are veneered by dm-thick thrombolitic crusts of clotted fabric (Fig. 5B, 16). On top of these pinnacles, a bed of more or less horizontal, platy non-skeletal stromatolites is developed, indicating lake-level lowstand conditions. Saline conditions are indicated by pseudomorphs of unidentified monoclinic-prismatic evaporite minerals. Non-skeletal stromatolites as well as thrombolites are rich in faecal pellets resembling that of the modern brine shrimp *Artemia*. Locally sickle-cell limestones form m-sized columns of stromatolitic appearance, e.g., at the stairway to the summit (Fig. 5C). At the eastern side below the summit, curtains of thin stalactites occur, reflecting early subaerial exposure already in Miocene times. On top of the castle rock, concentric structures of pinnacle cross-cuttings are visible.

Initially, spring mounds were considered as hot spring deposits of a Ries volcano (e.g., v. Gümbel 1870, Klähn 1926, Seemann 1935, 1941). However, after uncovering the impact origin of the Ries, artesian springs were favoured as cause of the „travertine" deposits. Wolff & Füchtbauer (1976) suggested that the Ries „travertines" are largely inorganic sinter limestones formed in early the history of the Ries lake by CO_2-degassing at subaerial springs discharging at concentrically arranged shear-planes of the inner crystalline ring.

Later, Bolten (1977) and Bolten & Gall (1978) proposed that the Wallerstein „travertines" formed, after an initial subaerial phase, submerged at a calcareous artesian spring discharging into a brackish lake. CO_2 degassing, rise in temperature and cyanobacterial activity were considered as driving mechanisms of $CaCO_3$ precipitation, although a comparison with tufa pinnacles of soda lakes was already drawn (Bolten 1977: 78). However, studies in present-day soda lakes indicate that tufa pinnacles similar to that of the Ries lake result from mixing of Ca^{2+}-supplying sublacustrine spring water and alkaline lake water (Arp et al. 1998, 1999). With regard to the Wallerstein, this interpretation is supported by $^{87}Sr/^{86}Sr$ isotope ratios that are shifted towards that of crystalline basement rocks, if compared to $^{87}Sr/^{86}Sr$ isotope ratios of algal bioherms (Fig. 16; Pache et al. 2001). On the other hand, stable oxygen and carbon isotope analyses

indicate that the CO_3^{2-} of the primary spring mound carbonates is largely derived from the lake water (Fig. 16).

The cyanobacterial biofilm, at first loosely $CaCO_3$ impregnated in such mixing zone, become successively lithified during shrinkage, bacterial degradation

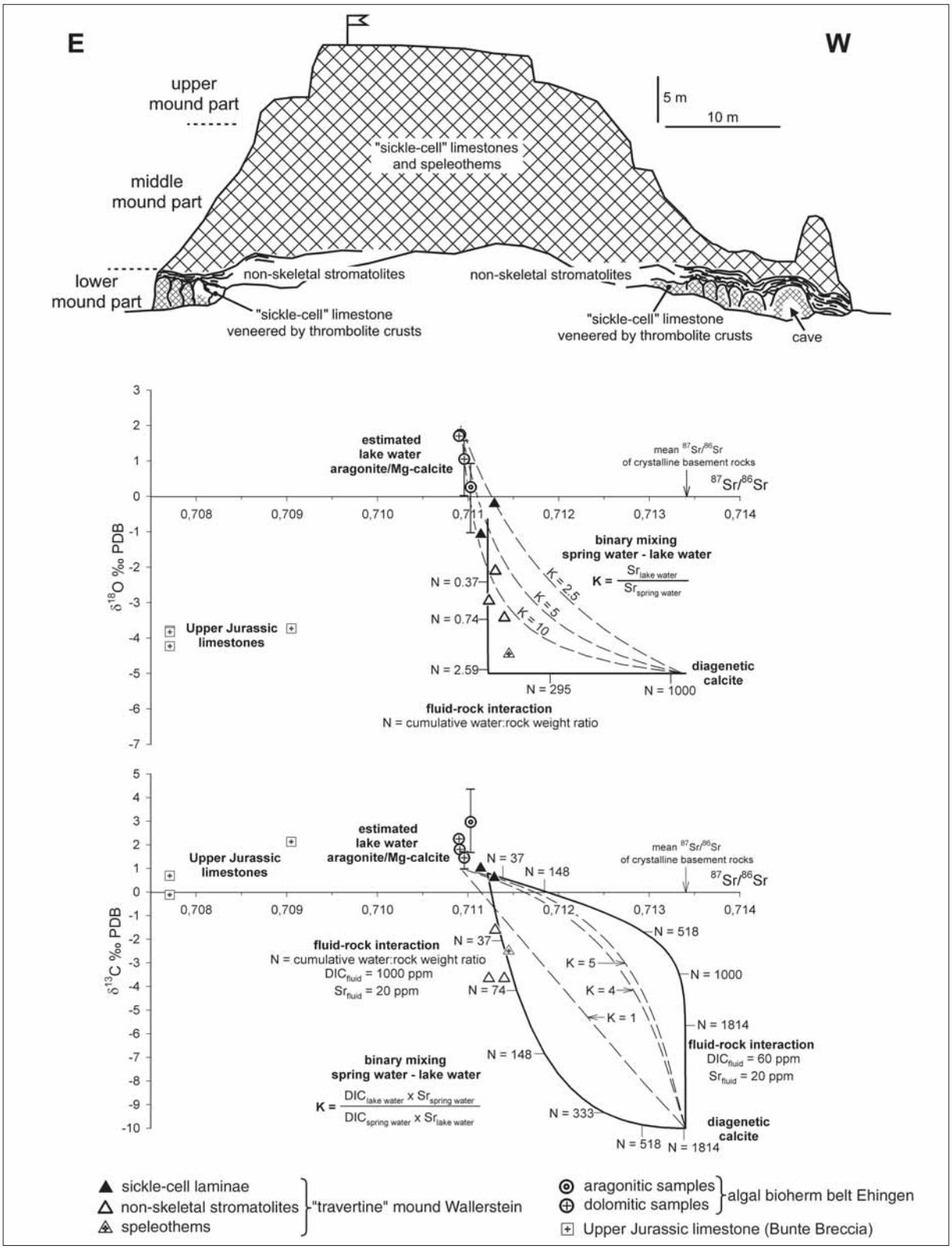

Fig. 16. Schematic section of the spring mound Wallerstein. Below, covariation plots of $d^{18}O$ vs. $^{87}Sr/^{86}Sr$ and $d^{13}C$ vs. $^{87}Sr/^{86}Sr$ of spring mound carbonates in comparison to algal bioherms and Upper Jurassic limestones are shown. Model curves demonstrate binary mixing of lake water and spring water from crystalline basement rocks (dashed lines) and fluid–rock interaction within the upwelling groundwater flow (solid lines). From Pache et al. (2001).

Fig. 17. The spring mound Alerheim castle rock located on the crystalline ring of the impact crater.

and secondary Ca^{2+} release from the biofilm exopolymers (Fig. 6; Arp et al. 1998). This mechanism sickle-cell fabric formation is only effective in highly alkaline water, i.e., soda lakes, buffering the simultaneously released CO_2 (Arp et al. 2003).

The Wallerstein carbonates are largely very poor in fossils, although avian eggshells and one tortoise have been reported (Deffner & Fraas 1877, Bolten 1977, Kohring & Sachs 1997). Such fossils appear to be restricted to pocket and fissure fillings of a freshwater phase younger than the true spring mound carbonates.

Stop 8: Alerheim castle rock (7129 Deiningen, east 43 98 330, north 54 11 730)

Together with the Wennenberg, Steinberg and Hahnenberg nearby, this conspicuous hill is part of the crystalline ring structure in the southeastern crater sector (Fig. 17). Located vis-à-vis the Wallerstein on the opposite site of the crater, the castle rock is another example of a large spring mound formed on a sublacustrine spring discharging from crystalline basement rocks (Bolten 1977). Similar to the Wallerstein castle rock, it is largely composed of sickle-cell limestones and associated speleothems. In addition, Nathan (1926) mentioned thin-bedded carbonates with ostracods from the western foot of the Alerheim castle rock. The castle rock is private property and to date poorly investigated.

Stop 9: Megesheim sand pit (7029 Oettingen, east 44 01 750, north 54 24 500)

The outcrop shows deltaic clastics of the Ries basin margin (Fig. 18). The brownish quartz sands and friable sandstones are part of the so-called „delta of Trendel“ (Bolten & Müller 1969). Years ago, almost 8 m of these deltaic sands were exposed in the sand pit (Chao et al. 1987). Large-scale foreset beds dipping 10° to 30° NNW are still visible (Fig. 18A) and point to a transport from crystalline rock areas further southeast (Chao et al. 1987, Hüttner et al. 1996). Indeed, layers of centimetre-sized crystalline rock pebbles are common. Upper Jurassic limestone clasts and kaolinized impact glass fragments are much more rare. In addition, few chalky, white-grey micrite beds up to 5 cm thick are intercalated.

After a discontinuity, one meter of dolomitic Hains-

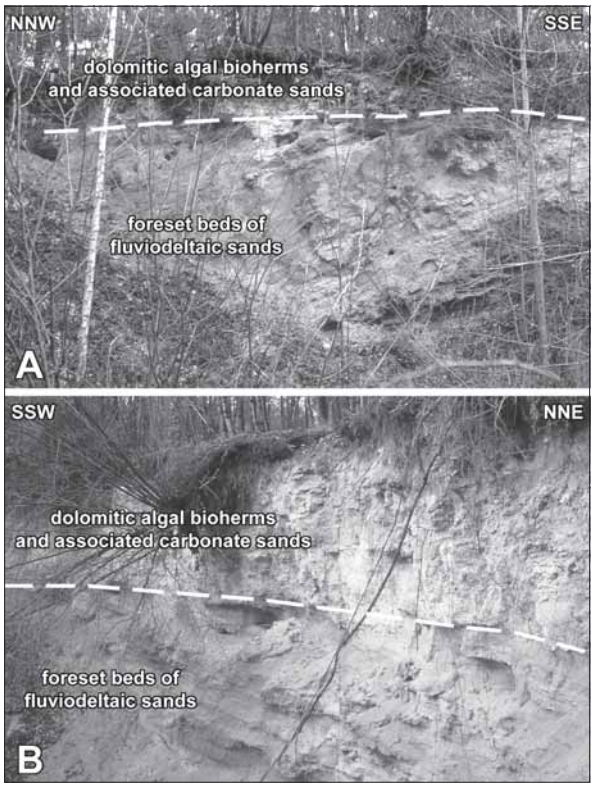

Fig. 18 A and B. Fluviodeltaic sands showing foreset beds are overlain by Hainsfarth-type dolomitic algal bioherms associated with peloidal carbonate sands. Sand pit Megesheim.

farth-type algal bioherms and associated carbonate sands form the top part of the outcrop (Fig. 18B). Bioherms are composed of sinter-veneered *Cladophorites*-bafflestones, while carbonate sands largely consist of peloids. These peloid-packstones contain intraclast layers, abundant *Hydrobia trochulus* and ostracods. Besides of *Strandesia risgoviensis*, rare *Eucypris* sp. and *Cypridopsis* have been found, too (Janz in Arp 1995b). Locally, root traces have been observed.

References

Andres, G. (1952): Eine Kalkalge aus dem Torton der südlichen Frankenalb. - Geologica Bavarica, 14: 41-47.

Armenat, M. (2003): Geologische Fazieskartierung der miozänen Kraterseesedimente am Südrand des Nördlinger Rieses (Süddeutschland). Gebiet Nördlingen-Herkheim-Schmähingen. - 58 pp., 1 map, Diplomkartierung Georg-August-Universität Göttingen.

Arp, G. (1995a): Ein Diplopode (Tausendfüßler i.e.S.) aus den lakustrinen Karbonaten des Nördlinger Rieses (Miozän, Süddeutschland): Morphologie und Integumentstruktur. - Paläontologische Zeitschrift, 69: 135-147.

Arp, G. (1995b): Lacustrine bioherms, spring mounds, and marginal carbonates of the Ries-impact-crater Miocene, Southern Germany). - Facies, 33: 35-90.

Arp, G. (1995c): Algenflora und Fazies der miozänen Karbonate am Nordrand des Kratersees im Nördlinger Ries (Süddeutschland). - Documenta naturae, 90: 1-197.

Arp, G. & Wiesheu, R. (1997): Ein kontinuierliches Profil von Algenbiohermen bis zu Seetonen des miozänen Rieskratersees: Sequenzen, Mikrofazies und Dolomitisierung. - Geologische Blätter für Nordost-Bayern, 47: 461-486.

Arp, G., Hofmann, J. & Reitner, J. (1998): Microbial fabric formation in spring mounds („microbialites“) of alkaline salt lakes in the Badain Jaran Sand Sea, PR China. - Palaios, 13: 581-592.

Arp, G., Thiel, V., Reimer, A., Michaelis, W. & Reitner, J. (1999): Biofilm exopolymers control microbialite formation at thermal springs discharging into the alkaline Pyramid Lake, Nevada, USA. - Sedimentary Geology, 126: 159-176.

Arp, G., Reimer, A. & Reitner, J. (2001): Photosynthesis-induced biofilm calcification and calcium concentrations in Phanerozoic oceans. - Science, 292: 1701-1704.

Arp, G., Reimer, A. & Reitner, J. (2003): Microbialite formation in seawater of increased alkalinity, Satonda Crater Lake, Indonesia. - Journal of Sedimentary Research, 73: 105-127.

Ballmann, P. (1979). Fossile Glareolidae aus dem Miozän des Nördlinger Ries (Aves : Charadriiformes). - Bonner zoologische Beiträge, 30: 51-101.

Ballmann, P. (1983). A new species of fossil barbet (Aves : Piciformes) from the late Miocene of the Nördlinger Ries (Southern Germany). Journal of Vertebrate Paleontology, 3: 43-48.

Barakat, A.O. & Rullkötter, J. (1997): A comparative study of molecular paleosalinity indicators: chromans, tocopherols and C_{20} isoprenoid thiophenes in Miocene lake sediments (Nördlinger Ries, southern Germany). - Aquatic Geochemistry, 3: 169-190.

Bayerisches Geologisches Landesamt (ed., 1969): Das Ries. Geologie, Geophysik und Genese eines Kraters. - Geologica Bavarica, 61: 1-478.

Bayerisches Geologisches Landesamt (ed., 1974): Die Forschungsbohrung Nördlinger 1973. - Geologica Bavarica, 72: 1-98.

Bayerisches Geologisches Landesamt (ed., 1977): Ergebnisse der Ries-Forschungsbohrung 1973: Struktur des Kraters und Entwicklung des Kratersees. - Geologica Bavarica, 75: 1-470.

Bolten, R.H. (1977): Die karbonatischen Ablagerungen des obermiozänen Kratersees im Nördlinger Ries. - 228 + 21 pp., 6 pls., Dissertation Universität München.

Bolten, R. & Gall, H. (1978): Der Wallersteiner Felsen - ein geologisches Phänomen. - Nordschwaben, 6: 18-21.

Bolten, R. & Müller, D. (1969): Das Tertiär im Nördlinger Ries und in seiner Umgebung. - Geologica Bavarica, 61: 87-130.

Bolten, R.H., Gall, H. & Jung, W. (1976): Die obermiozäne (sarmatische) Fossil-Lagerstätte Wemding im Nördlinger Ries (Bayern). Ein Beitrag zur Charakterisierung des Riessee-Biotops. - Geologische Blätter für NO-Bayern, 26: 75-94.

Cabrol, N.A., Wynn-Williams, D.D., Crawford, D.A. & Grin, E.A. (2001): Recent aqueous environments in Martian impact craters: An astrobiological perspective. - Icarus, 154: 98–112.

Chao, E.T.C. & Littler, J. (1963) Additional evidence for the impact origin of the Ries basin, Bavaria, Germany. - Geological Society of America Special Paper, 73: 127.

Chao, E.T.C. (1977): The Ries crater of southern Germany, a model for large basins on planetary surfaces. - Geologisches Jahrbuch, A 43: 3-81.

Chao, E.T.C., Hüttner, R. & Schmidt-Kaler, H. (1987): Aufschlüsse im Ries-Meteoriten-Krater. - 84 pp., München (Bayerisches Geologisches Landesamt)

Cockell, C.S. & Lee, P. (2002): The biology of impact craters: A review. - Biological Reviews, 77: 279-310.

Deffner, C. & Fraas, O. (1877): Begleitworte zur geognostischen Spezialkarte von Württemberg. Atlasblätter Bopfingen und Ellenberg. - 36 pp., Stuttgart.

Dehm, R., Gall, H., Höfling, R., Jung, W. & Malz, H. (1977): Die Tier- und Pflanzenreste aus den obermiozänen Riessee-Ablagerungen in der Forschungsbohrung Nördlingen 1973. - Geologica Bavarica, 75: 91-109.

Diemand, A. (1898): Der Wallersteiner Felsen und seine Geschichte. - 76 pp., Nördlingen (Reischle).

El Goresy, A., Chen, M., Dubrovinsky, L., Gillet, P. & Graup, G. (2001): An ultradense polymorph of rutile with seven-coordinated titanium from the Ries crater. - Science, 293: 1467-1470.

Ernstson, K. & Pohl, J. (1977): Neue Modelle zur Verteilung der Dichte und Geschwindigkeit im Ries-Krater. - Geologica Bavarica, 75: 355-371.

Freytet, P. & Plaziat, J.C. (1982): Continental carbonate sedimentation and pedogenesis - Late Cretaceous and Early Tertiary of Southern France. - Contributions to Sedimentology, 12: 1-213.

Füchtbauer, H., von der Brelie, G., Dehm, R., Förstner, U.,

Gall, H., Höfling, R., Hoefs, J., Hollerbach, H., Jankowski, B., Jung, W., Malz, H., Mertes, H., Rothe, P., Salger, M., Wehner, H. & Wolf, M. (1977): Tertiary lake sediments of the Ries, research borehole Nördlingen 1973 - a summary. - Geologica Bavarica, 75: 13-19.

Gall, H., Müller, D. & Stöffler, D. (1975): Verteilung, Eigenschaften und Entstehung der Auswurfmassen des Impaktkraters Nördlinger Ries. - Geologische Rundschau, 64: 915-947.

Gentner, W. & Wagner, G.A. (1969): Altersbestimmung an Riesgläsern und Moldaviten. - Geologica Bavarica, 61: 296-303.

Gorthner, A. (1992): Bau, Funktion und Evolution komplexer Gastropodenschalen in Langzeit-Seen. Mit einem Beitrag zur Paläobiologie von *Gyraulus „multiformis“* im Steinheimer Becken. - Stuttgarter Beiträge zur Naturkunde, B 190: 1-173.

Grey, K., Moore, L.S., Burne, R.V., Pierson, B.K. & Bauld, J. (1990): Lake Thetis, Western Australia: an example of saline lake sedimentation dominated by benthic microbial processes. - Australian Journal of Marine and Freshwater Research, 41: 275-300.

Groiss, J.T. (1974): Konglomerat-Bildungen an der Auflagerung von tertiärem Süßwasserkalk auf Grundgebirge am nördlichen Riesrand. - Geologische Blätter für Nordost-Bayern, 24: 279-285.

Groiss, J.T., Haunschild, H. & Zeiss, A. (2000): Das Ries und sein Vorland. - Sammlung Geologischer Führer, 92: 271 pp., Stuttgart (Borntraeger).

Heizmann, E.P.J. & Fahlbusch, V. (1983): Die mittelmiozäne Wirbeltierfauna vom Steinberg (Nördlinger Ries). Eine Übersicht. - Mitteilungen der Bayerischen Staatssammlung für Paläontologie und historische Geologie, 23: 83-93.

Heizmann, E.P.J. & Hesse, A. (1995). Die mittelmiozänen Vogel- und Säugetierfaunen des Nördlinger Ries (MN6) und des Steinheimer Beckens (MN7) - ein Vergleich. - Courier Forschungsinstitut Senckenberg, 181: 171-185.

Hilgendorf, F. (1866): *Planorbis multiformis* im Steinheimer Süsswasserkalk. Ein Beispiel von Gestaltveränderung im Laufe der Zeit. - 36 pp., Berlin (Buchhandlung W. Weber.

Höfling, R. (2003) Das Nördlinger Ries und sein Vorland aus sedimentologisch-paläontologischer Sicht (Exkursion G am 25. April 2003). - Jahresberichte und Mitteilungen des oberrheinischen geologischen Vereins, Neue Folge, 85: 203-239.

Hollaus, E. (1969): Geologische Untersuchungen im Ries. Das Gebiet der Blätter Nördlingen-Ost und Nördlingen-West, mit besonderer Berücksichtigung der Pleistozän-Ablagerungen. - 85 pp., Dissertation Universität München

Hough R.M., Gilmour I., Pillinger C.T., Arden J.W., Gilkes K.W.R., Yuan Y. & Milledge H.J. (1995): Diamond and silicon carbide in impact melt rock from the Ries impact crater. - Nature, 378: 41-44.

Hüttner, R. & Schmidt-Kaler, H. (1999): Die Geologische Karte des Rieses 1:50 000 (2. überarbeitete Auflage). Erläuterungen zu Erdgeschichte, Bau und Entstehung des Kraters sowie zu den Impaktgesteinen. - Geologica Bavarica, 104: 7-76.

Hüttner, R. (1969): Bunte Trümmermassen und Suevit. - Geologica Bavarica, 61: 142-200.

Hüttner, R. (1977): Impaktgesteine des Rieses. - Geologica Bavarica, 76: 108-175.

Hüttner, R., Pösges, G., Reiff, W. & Schieber, M. (1996): Nördlinger Ries und Steinheimer Becken. - Zeitschrift für geologische Wissenschaften, 24: 121-139.

Jankowski, B. (1977): Die Postimpakt-Sedimente in der Forschungsbohrung Nördlingen 1973. - Geologica Bavarica, 75: 21-36.

Jankowski, B. (1981): Die Geschichte der Sedimentation im Nördlinger Ries und Randecker Maar. - Bochumer geologische und geotechnische Arbeiten, 6: 1-315.

Janz, H. (1995): Neubeschreibung von *Strandesia risgoviensis* nov. comb. (Sieber 1905) (Crustacea, Ostracoda) aus dem Nördlinger Ries (Miozän, Süddeutschland). - Stuttgarter Beiträge zur Naturkunde, B 233: 1-17.

Kavasch, J. (1985): Meteoritenkrater Ries. Ein geologischer Führer. 7th ed. - 88 pp., Donauwörth.

Kempe, S., Kazmierczak, J, Landmann, G., Konuk, T., Reimer, A. & Lipp, A. (1991): Largest known microbialites discovered in Lake Van, Turkey. - Nature, 349: 605-608.

Klähn, H. (1926): Vergleichende paläolimnologische, sedimentpetrographische und tektonische Untersuchungen an miocänen Seen der Schwäbischen Alb. - Neues Jahrbuch für Mineralogie, Geologie und Paläontologie, Abteilung B, 55: 274-428.

Klappa, C.F. (1978): Biolithogenesis of *Microcodium*: elucidation. - Sedimentology, 25: 489-522.

Knollmann, S. (2003): Fazieskartierung der miozänen Seesedimente im Gebiet Megesheim-Trendel-Ursheim (Nördlinger Ries, Süddeutschland). - 60 pp., 1 map, Diplomkartierung Georg-August-Universität Göttingen.

Kohring, R. & Sachs, O. (1997): Erhaltungsbedingungen und Diagenese fossiler Vogeleischalen aus dem Nördlinger Ries (Miozän, MN6). - Archaeopteryx, 15: 73-96.

Lemcke, K. (1981): Das Nördlinger Ries: Spur einer kosmischen Katastrophe. - Spektrum der Wissenschaft, 1: 110-121.

Margolin, P. (2000): The Making of Lunar Explorers. - Geotimes, 45 (8): 18-21.

Mensink, H. (1984): Die Entwicklung der Gastropoden im miozänen See des Steinheimer Beckens. - Palaeontographica, A 183: 1-63.

Mertes, H. (1977): Rutschgefüge in den jungtertiären See-Sedimenten der Forschungsbohrung Nördlingen 1973. - Geologica Bavarica 75: 75-89.

Metz, R. (ed., 1974): Das Nördlinger Ries. Beiträge zur Geologie und Mineralogie von Einschlagkratern. Der Aufschluss, Sonderheft, 24: 1-94.

Mayr, G. & Göhlich, U.B. (2004): A new parrot from the Miocene of Germany, with comments on the variation of hypotarsus morphology in some Psittaciformes. - Belgian Journal of Zoologie, 134: 47-54.

Moore, L.S. (1987): Water chemistry of the coastal saline Lakes of the Clifton-Preston Lakeland System, Southwestern Australia, and its influence on stromatolite formation.- Australian Journal of Marine and Freshwater Research, 38: 647-660.

Nathan, H. (1925): Geologische Untersuchungen im Ries.

Das Gebiet des Blattes Möttingen. - Neues Jahrbuch für Mineralogie, Geologie und Paläontologie, Beilage-Band, 53 (Abt. B): 31-97.

Nathan, H. (1935): Geologische Untersuchungen im Ries. Das Gebiet des Blattes Ederheim. - Abhandlungen der geologischen Landesuntersuchung am Bayerischen Oberbergamt, 19: 1-42.

Nathan, H. (1957): Wasserbohrungen im Ries. - Geologisches Jahrbuch, 74: 135-146.

Osinski, G.R., Lee, P., Spray, J.G., Parnell, J., Lim, D.S.S., Bunch, T.E., Cockell, C.S. & Glass, B. (2005): Geological overview and cratering model for the Haughton impact structure, Devon Island, Canadian High Arctic. - Meteoritics & Planetary Science, 40: 1759-1776.

Pache, M. (2000): Mikrofazies und Geochemie des miozänen Spring Mounds Wallerstein (Nördlinger Ries, Süddeutschland). Fazieskartierung der Miozänsedimente im Gebiet Maihingen-Utzwingen-Herblingen (Nördlinger Ries, Süddeutschland. - 97 + 5 pp., 1 map, Diplomarbeit und Diplomkartierung Georg-August-Universität Göttingen.

Pache, M., Reitner, J. & Arp, G. (2001): Geochemical evidence for the formation of a large Miocene „travertine“ mound at a sublacustrine spring in a soda lake (Wallerstein castle rock, Nördlinger Ries, Germany). - Facies, 45: 211-230.

Peters, H. (2003): Faziesverteilung und Dolomitisierung der Karbonatsedimente des Rieskratersees im Gebiet Oettingen i. Bay. - Hainsfarth (Miozän, Süddeutschland). - 323 pp., 70 plates, 2 maps, Diplomarbeit und -kartierung Georg-August-Universität Göttingen.

Pohl, J. & Gall, H. (1977): Bau und Entstehung des Ries-Kraters. - Geologica Bavarica, 76: 159-175.

Pösges, G. & Schieber, M. (1997): The Ries Crater Museum Nördlingen. - 80 pp., München (Pfeil)

Rachl, R. (1983): Die Chiroptera (Mammalia) aus den mittelmiozänen Kalken des Nördlinger Rieses (Süddeutschland). - 284 pp., Dissertation Ludwig-Maximilians-Universität München.

Reich, H. & Horrix, W. (1955): Geophysikalische Untersuchungen im Ries und Vorries und deren geologische Bedeutung. - Beiheft zum Geologischen Jahrbuch, 19: 1-119.

Reis, O.M. (1926): Zusammenfassung über die im Ries südlich von Nördlingen auftretenden Süßwasserkalke und ihre Entstehung. - Jahresberichte und Mitteilungen des Oberrheinischen Geologischen Vereins, Neue Folge, 14 (1925): 176-190.

Riding, R. (1979): Origin and diagenesis of lacustrine algal bioherms at the margin of the Ries crater, Upper Miocene, southern Germany. - Sedimentology, 26: 645-680.

Riding, R. (1991): Classification of microbial carbonates. - In: Riding, R. (ed.): Calcareous algae and stromatolites: 21-51, Berlin (Springer)

Rothe, P. & Hoefs, J. (1977): Isotopen-geochemische Untersuchungen an Kabonaten der Ries-See-Sedimente der Forschungsbohrung Nördlingen 1973. - Geologica Bavarica, 75: 59-66.

Rullkötter, J., Littke, R. & Schäfer, R.G. (1990) Characterization of organic matter in sulfur-rich lacustrine sediments of Miocene age (Nördlinger Ries, southern Germany). - In Orr, W.L. & White, C.M. (eds.): Geochemistry of Sulfur in Fossil Fuels. - American Chemical Society Symposium Series, 249: 149-169.

Russel, I.C. (1889): Quarternary history of the Mono Valley, California. - Eighth Annual Report of the United States Geological Survey: 262-394, Lee Vining (Reprint 1984, Artemisia Press)

Schauderna, H. (1983): Die Diatomeenflora aus den Miozänen Seeablagerungen im Nördlinger Ries. - Palaeontographica, B 188: 83-193.

Schieber, M. (2002): Die Meteoritenkrater Nördlinger Ries und Steinheimer Becken. - In: Niebuhr, B. (ed.): GEO 2002 Planet Erde: Vergangenheit, Entwicklung, Zukunft. 1.-5. Oktober 2002 in Würzburg, Exkursionsführer. Schriftreihe der Deutschen Geologischen Gesellschaft, Heft 22: 33-44.

Schieber, M. (2004): Aspekte des Geotourismus im Meteoritenkrater Nördlinger Ries. - Der Aufschluss, 55: 247-255.

Scholl, D.W. & Taft, W.H. (1964): Algae, contributors to the formation of calcareous tufa, Mono Lake, California. - Journal of Sedimentary Petrology, 34: 309-319.

Schröder, J. & Dehm, R. (1950): Geologische Untersuchungen im Ries. Das Gebiet des Blattes Harburg. - Abhandlungen des Naturwissenschaftlichen Vereins für Schwaben e. V., 5: 1-147.

Seemann, R. (1935): Massenhaftes Auftreten von Insektenpuppen im obermiozänen Süßwasserkalk vom Goldberg im Ries. - Jahreshefte des Vereins für vaterländische Naturkunde in Württemberg, 91: 19-21.

Seemann, R. (1941): Geologische und palaeofaunistische Untersuchungen am Goldberg im Ries. - Jahreshefte des Vereins für vaterländische Naturkunde in Württemberg 96 (Jahrgang 1940), Teil IV: 49-62.

Shoemaker, E.M. & Chao, E.C.T. (1961): New evidence for the impact origin of the Ries basin, Bavaria, Germany. - Journal of Geophysical Research, 66: 3371-3378.

Staudacher, T., Jessberger, E.K., Dominik, B., Kirsten, T. & Schaeffer, O.A. (1982): ^{40}Ar-^{39}Ar ages of rocks and glasses from the Nördlinger Ries crater and the temperature history of impact breccias. - Journal of Geophysics, 51: 1-11.

Steinert, H. (1974): 1200 Meter tief in den Krater bei Nördlingen. - Kosmos 70: 353-356.

Stöffler D. & Ostertag R. (1983): The Ries impact crater. - Fortschritte der Mineralogie 61, Beiheft 2: 71-116.

Stöffler, D. (1977): Research drilling Nördlingen 1973: polymict breccias, crater basement, and cratering model of the Ries impact structure. - Geologica Bavarica, 75: 443-458.

Sumner, D.Y. (1997) Late Archean calcite-microbe interactions: two morphologically distinct microbial communities that affected calcite nucleation differently. - Palaios, 12: 302-318.

von Gümbel, C.W. (1870): Über den Riesvulkan und über vulkanische Erscheinungen im Rieskessel. - Sitzungsberichte der königlich-bayerischen Akademie der Wissenschaften, mathematisch-physikalische Classe, 1 (Heft 2): 153-200.

von Gümbel, C.W. (1889): Kurze Erläuterung zum Blatte Nördlingen (No. XVI) der geognostischen Karte des Königreichs Bayern. - 43 pp., Cassel (Fischer)

von Gümbel, C.W. (1891): Geognostische Beschreibung der Fränkischen Alb (Frankenjura) mit dem anstos-

senden fränkischen Keupergebiet.- Geognostische Beschreibung des Königreichs Bayern. Vierte Abtheilung: 763 pp., Kassel (Fischer)

Weber, E. (1941): Geologische Untersuchungen im Ries. Das Gebiet des Blattes Wemding. - Abhandlungen des Naturkunde- und Tiergartenvereins für Schwaben e.V., 3 (geol.-paläont. Reihe, 2. Heft): 1-248.

Wolf, M. (1977): Kohlenpetrographische Untersuchungen der See-Sedimente der Forschungsbohrung Nördlingen 1973 und Vergleich mit anderen Untersuchungsergebnissen aus dem Ries. - Geologica Bavarica, 75: 127-138.

Wolff, M. & Füchtbauer, H. (1976): Die karbonatische Randfazies der tertiären Süßwasserseen des Nördlinger Ries und des Steinheimer Beckens. - Geologisches Jahrbuch, D 14: 3-53.

Ziegler, R. (1983): Odontologische und osteologische Untersuchungen an *Galerix exilis* (Blainville) (Mammalia, Erinaceidae) aus den miozänen Ablagerungen vom Steinberg und Goldberg im Nördlinger Ries (Süddeutschland). - 244 pp., Dissertation Ludwig-Maximilians-Universität München.